2007

Construction and application of computationally tractable theories on nonlinear spectroscopy

Christine L. Neipert
University of South Florida

Construction and Application of Computationally Tractable Theories of Nonlinear Spectroscopy

by

Christine L. Neipert

A dissertation submitted in partial fulfillment
of the requirements for the degree of
Doctor of Philosophy
Department of Chemistry
College of Arts and Sciences
University of South Florida

Major Professor: Brian Space, Ph.D.
Alfredo Cardenas, Ph.D.
Randy Larsen, Ph.D.
Lilia Woods, Ph.D.

Date of Approval:
May 23, 2007

Keywords: water, molecular dynamics, liquid/vapor interface, nonlinear spectroscopy, SFG

Acknowledgments

I would like to express my gratitude to my husband, Mike. His love and guidance have been blessings in my life. The unwavering support he has offered and his belief in me has been a true source of joy and inspiration in my life. I extend my deepest and most sincere gratitude, and only hope that my support of him continues to be as meaningful as what he has given to me.

My thanks also go out to my current and former group members: Dr. Russell DeVane, Dr. Christina Kasprzyk, Dr. Angela Perry, Dr. A. Ben Roney, Mr. Jon Belof, Mr. Tony Green, Ms. Ashley Mullen, and Mr. Abe Stern. They have been wonderful friends and colleagues.

Many thanks also to Professor Preston Moore, whose help and advice has been invaluable. I would also like to thank my committee: Dr. Alfredo Cardenas, Dr. Randy Larsen, and Dr. Lilia Woods.

Finally, over the past four years, I have been guided and mentored by a remarkable person, Professor Brian Space. In everyone's life, there are those few people who hold special significance; Professor Space has opened up a world of opportunity to me, and has been one of the most positive influences in my life. Words or deeds cannot possibly begin to express my gratitude, and the deep respect that I have for him. I offer my humblest thank you.

Note to Reader

Note to Reader: The original of this document contains color that is necessary for understanding the data. The original dissertation is on file with the USF library in Tampa, Florida.

Table of Contents

List of Figures

List of Tables

Construction and Application of Computationally Tractable Theories of Nonlinear Spectroscopy

Christine L. Neipert

ABSTRACT

Nonlinear optical processes probe systems in unique manners. The signals obtained from nonlinear spectroscopic experiments are often significantly different than more standard linear techniques, and their intricate nature can make it difficult to interpret the experimental results. Given the complexity of many nonlinear lineshapes, it is to the benefit of both the theoretical and experimental communities to have molecularly detailed computationally amenable theories of nonlinear spectroscopy. Development of such theories, bench marked by careful experimental investigations, have the ability to understand the origins of a given spectroscopic lineshape with atomistic resolution. With this goal in mind, this manuscript details the development of several novel theories of nonlinear surface specific spectroscopies.

Spectroscopic responses are described by quantum mechanical quantities. This work shows how well defined classical limits of these expressions can be obtained, and unlike the formal quantum mechanical expressions, the derived expressions comprise a computationally tractable theory. Further, because the developed novel theories have a well defined classical limit, there is a quantum classical correspondence. Thus, semiclassical computational techniques can capture the true physics of the given nonlinear optical pro-

cess. The semiclassical methodology presented in this manuscript consists of two primary components – classical molecular dynamics and a spectroscopic model. For each theory of nonlinear spectroscopy that is developed, a computational implementation methodology is discussed and/or tested.

Chapter 1

Introduction

The interaction of light and matter. Seemingly simple, the true complexity of this interaction was beginning to be realized as early as 300 B.C. with the work of Euclid. Names such as Kepler, Newton, Maxwell, and Einstein dot the landscape in the evolution of this scientific frontier. [1, 2] The culmination of this work lead to a significant technological innovation in the mid-twentieth century: the development of the first contemporary laser, and in turn, the field of modern optical spectroscopy. [2–5]

Modern optical spectroscopic techniques are powerful tools for probing the structure and dynamics of molecular systems. [2–16] This is well illustrated by comparing a given system's gas and condensed phase spectra. Condensed phase spectra can show, *e.g.*, shifts in fundamental resonant frequencies in comparison to their gas phase spectra, and/or exhibit such effects as motional narrowing. The differences between the spectra of the two phases are due to the many-body effects that are present in the condensed phase and that are absent in the gas phase. Further, studying spectroscopy from a theoretical perspective is enticing because the underlying molecular interactions probed by a specific type of spectroscopy can be realized with proper analysis and comparison to experiment. [6, 17–19]

Beginning with the pioneering, and now famous, work of Bloembergen, [20–23] Gordon, [24–29] and many others in the mid-twentieth century, talented scientists have been

constructing theories of linear and nonlinear spectroscopy. This body of work continues on in that tradition, but using a new, unique, approach which is amenable to semiclassical computation techniques. In Chapter 2, the general theory of spectroscopy is presented and discussed. In subsequent chapters, theories which use the general formalism, detailed in Chapter 2, as the starting point in their construction are presented and discussed – these include: dipolar sum vibrational frequency spectroscopy (SVFS), multi-polar SVFS, and third order SVFS. In the final chapter preceding the concluding remarks, the novel approach used to describe various SVFS processes is applied to develop the well known Optical Kerr Effect (OKE) result. This is done to make a connection with the more common Louiville space approach, and explicitly express the implicit assumptions that are present in these other techniques.

Chapter 2

Theoretical Background

2.1 Generalized Density Matrix Theory Approach

In typical electric optical laboratory experiments, a light field is impinged on a system, and the resulting polarization, $\boldsymbol{P}$, is measured. [2] Letting M denote the number of system molecules, $\boldsymbol{\mu}$ the system dipole moment operator, and a set of angle brackets a quantum mechanical expectation value, the relationship between the measured polarization and system dipole moment operator is given by:

$$\boldsymbol{P} = M\overline{\langle \boldsymbol{\mu} \rangle} = M\langle \boldsymbol{\mu}\rho \rangle \tag{2.1}$$

In the first part of this equality, the bar indicates the quantum mechanical expectation value is to be further ensemble averaged. This secondary average is taken because of our inability to determine the exact many-body wavefunction of the system as it evolves in time. [2, 4–6] (This inability is a pure classical statistical phenomenon as opposed to an inherent uncertainty due to quantum mechanical constraints.) In the second portion of the equality in Equation 2.1, the density matrix, ρ, has been incorporated to account for this statistical uncertainty. Formally, the density matrix between states n and m is given by:

$$\rho_{mn} = \sum_s p(s)\ a_m^{*(s)}(t) a_n^{(s)}(t) \tag{2.2}$$

Here, $p(s)$ denotes the probably of the system being in state s and the $a^{(s)}$ coefficients are time dependent probability amplitudes in standard fashion. In the limit the exact state of the wavefunction were known, the distribution $p(s)$ would reduce to a delta function, and Equation 2.1 would simplify to a typical non-ensemble averaged expectation value.

As a system evolves in time under the influence of a perturbation, the wavefunction changes. This evolution is formally described by the time dependent Schrödinger equation. [30] Inclusion of the classical statistical uncertainty in this equation results in an equation of motion for the density matrix:

$$\frac{d\rho_{nm}}{dt} = \frac{i}{\hbar}[\rho, H_T]_{nm} \tag{2.3}$$

Here, H_T denotes the total many-body Hamiltonian of the system. It is common to further partition Equation 2.3 into two pieces to facilitate theoretical development.

$$\frac{d\rho_{nm}}{dt} = \frac{i}{\hbar}[\rho, H]_{nm} - \gamma_{nm}(\rho_{nm} - \rho_{nm}^{(eq)}) \tag{2.4}$$

In Equation 2.4, interactions, such as atomic collisions, that are not easily mathematically incorporated into the Hamiltonian and contribute to the system's decay, are separated out. [2, 4] These interactions are represented by the second term in Equation 2.4. Here, $\gamma_{nm} = \gamma_{mn}$ and is a phenomenological, purely real, damping factor that weights how quickly the system will relax back to the equilibrium density matrix value when, *e.g.*, an atomic collision occurs. Generally, this equation of motion cannot be solved analytically, but can be expanded in a power series and solved order by order. To proceed in the derivation, it is further assumed that: (1) the Hamiltonian, H, is separable into equilibrium and perturbed components ($H = H^{(o)} + H^{(1)}$), and (2) $\rho_{nm}^{(0)} = \begin{cases} \rho_{nm}^{(eq)} & n = m \\ 0 & n \neq m \end{cases}$. In essence, (2) constrains the proscribed mathematical description to a system in which any state that is occupied in equilibrium must be in a population, and further requires that any excitation does not produce a coherent superposition of states. [2]

Proceeding with an ordered expansion of the density matrix such that a solution can be used to solve for the primary quantity of interest – the polarization (Equation 2.1):

$$\frac{d\rho_{nm}}{dt} = \sum_i \frac{d\rho_{nm}^{(i)}}{dt} = \frac{i}{\hbar} \sum_i \left\{ [\rho^{(i-1)}, H^{(1)}]_{nm} - E_{nm}\rho_{nm}^{(i)} - i\gamma_{nm}(\rho_{nm}^{(i)} - \rho_{nm}^{(eq)}) \right\} \quad (2.5)$$

Here, E_{nm} is defined as $E_n - E_m$, and is the energy difference between states n and m. Also, note that for $i = 0$, the commutator in Equation 2.5 must be zero because the zeroth order density matrix describes the system in equilibrium – *i.e.* prior to the perturbation, $H^{(1)}$.

Solving the density matrix equation of motion in a perturbative manner facilitates writing the observed polarization in terms of an ordered expansion also:

$$\boldsymbol{P} = \sum_N \boldsymbol{P}^{(N)} = M \sum_{N=0} \langle \boldsymbol{\mu} \rho^{(N)} \rangle \quad (2.6)$$

Equation 2.6 can provide further physical insight by considering that the specific phase and intensity of the detected polarization will depend on the intrinsic response function of the system as well as the properties of the applied perturbing field(s). By definition, a system's intrinsic response function provides a complete description of it under all conditions. (The label of response function is generally used to describe this quantity in the time domain. However, in the frequency domain, the response is typically referred to as the susceptibility, $\boldsymbol{\chi}$.) In pursuit of this physical insight, consider a general perturbing electric field (that may or may not be the only perturbing field) applied at time t and position $\mathbf{r}$:

$$\mathbf{E}(\mathbf{r}, t) = \sum_n^{N_F} \left(\mathbf{E}_n(\mathbf{t}) e^{i\mathbf{k_n}\cdot\mathbf{r}} + \mathbf{E}_n^*(\mathbf{t}) e^{-i\mathbf{k_n}\cdot\mathbf{r}} \right) \quad (2.7)$$

In Equation 2.7, $\mathbf{k_n}$ is the wave vector specifying the electric field's propagation direction, and components that are slowly varying in space and those that are spatially highly oscillatory have been partitioned. [3, 5, 31] The slowly varying spacial component, $\mathbf{E_n}(t)$,

can generally be further decomposed into temporally ($\epsilon_n(t)$) and spatially ($\mathbf{E}_n$) dependent parts. [31] This subsequent separation allows the field to be rewritten in the form:

$$\mathbf{E}(\mathbf{r},t) = \sum_{n}^{N_F} \left(\mathbf{E}_n \epsilon_n(t) e^{i\mathbf{k_n}\cdot\mathbf{r}} + \mathbf{E}_n^* \epsilon_n^*(t) e^{-i\mathbf{k_n}\cdot\mathbf{r}} \right) \tag{2.8}$$

In Equations 2.7 and 2.8, the sum on n ranges over the number of applied perturbing fields (N_F), and is included because, in the most general case, exact time ordering of multiple applied fields cannot be assumed. [5] In practice, experiments in the time domain typically use relatively short pulses that are separated and ordered in time while the frequency domain techniques employ nearly monochromatic laser fields that overlap in time and space – such considerations simplify the required analysis considerably. Given the definition of the field in Equation 2.8, the most general description of the N^{th} component of the polarization (Equation 2.6), takes the form of a multiple time integration over the N^{th} order material response function, $\mathbf{R}^{(N)}$:

$$\mathbf{P}^{(N)}(\mathbf{r},t) = \int_0^\infty d\tau_1 \cdots \int_0^\infty d\tau_N \; \mathbf{R}^{(N)}(\tau_1,\cdots,\tau_N) \mid \mathbf{E}(\mathbf{r},t-\tau_1)\cdots\mathbf{E}(\mathbf{r},t-\tau_N) \tag{2.9}$$

Here, $\mathbf{R}^{(N)}$ is an $(N+1)$ ranked tensor, and the $\mid$ represents N tensor contractions. In this rewrite of the polarization, it should not be overlooked that $\mathbf{R}^{(N)}$ is a quantum mechanical object which is order $\hbar^N$ dependent and is a function of the perturbed Hamiltonian operator. In Equation 2.9, the time integrations are necessary to account for the fact that there will be a time delay between application of the field(s) and the response of the system. [6,32,33] If both processes were simultaneous, the integrations would not be necessary. This simultaneous field application/system response limit is commonly referred to as the delta function pulse limit, and while it is not strictly ever true, it is often assumed from a theoretical standpoint to simplify calculation of the polarization. [5] Unlike the delta function pulse limit, the analogous limit in frequency space is not unphysical because while a true delta function pulse is not achievable, a nearly monochromatic field

is. [3, 5] In the limit of monochromatic fields, $\boldsymbol{E}(\omega_i) = 2\pi \boldsymbol{E}_i \delta(\omega_i - \Omega_i)$ and the N^{th} order total polarization expressed as a frequency Ω is given by a simple equality: [6]

$$\mathbf{P}^{(N)}(\mathbf{r}, \Omega) = (2\pi)^{N-1} \boldsymbol{\chi}^{(N)}(\omega_1 ... \omega_N) \mid \mathbf{E}_1 \delta(\omega_1 - \Omega_1) ... \mathbf{E}_N \delta(\omega_N - \Omega_N) \tag{2.10}$$

Equation 2.10 describes the total N^{th} order polarization a given sample emits when optically perturbed by N total interactions with a single or several monochromatic electric fields. However, it is not necessarily common to measure the total N^{th} order polarization because there are unique optical processes that contribute to the total N^{th} order polarization, and can be detected independently. This later method is advantageous because more information regarding the system can be realized by analyzing each contribution to the total polarization independently. Specifically, insertion of Equation 2.8 into Equation 2.9 implies there are $(2N_F)^{N_F}$ terms present for each $\mathbf{P}^{(N)}(\mathbf{r}, \Omega)$ component. Each of the $(2N_F)^{N_F}$ terms represent a distinct optical process that is radiated in a specific direction and frequency determined by combinations of the incident fields' wave vectors and frequencies. (Note, a field's frequency and wave vector are directly related, and by convention, possess the same sign.) For example, consider two perturbing fields where the response is not instantaneous. From Equation 2.8, and letting $c.c.$ represent a given term's complex conjugate, it follows that the fields are formally expressed as:

$$\mathbf{E}(\mathbf{r}, t - \tau_1) = \mathbf{E}_1(t - \tau_1) e^{i\mathbf{k_1} \cdot \mathbf{r}} + c.c. + \mathbf{E}_2(t - \tau_1) e^{i\mathbf{k_2} \cdot \mathbf{r}} + c.c. \tag{2.11}$$

$$\mathbf{E}(\mathbf{r}, t - \tau_2) = \mathbf{E}_1(t - \tau_2) e^{i\mathbf{k_1} \cdot \mathbf{r}} + c.c + \mathbf{E}_2(t - \tau_2) e^{i\mathbf{k_2} \cdot \mathbf{r}} + c.c. \tag{2.12}$$

If the product of these two fields is taken (Equation 2.6), 16 terms result. These are summarized in Table 2.1. Table 2.1 also serves to further reinforce that specific combinations of the applied fields' wave vectors will result in unique polarization signals

which are emitted from the sample in highly specific directions. The detected signal from a specific optical process detected a frequency ω_s and wave vector $\mathbf{k_s}$ is denoted by $\boldsymbol{P}^{(N)}(\mathbf{k_s}, \omega_s)$, and the sum of all the polarization signals (16 in this case) is the total polarization, $\boldsymbol{P}^{(N)}(\mathbf{r}, \Omega)$.

Now, consider a single perturbing field that is not sufficiently intense in the sense that it would not invalidate the perturbative description that has been developed thus far. In this case – neglecting the zeroth order term from here on because it is a constant corresponding to an unperturbed system – the series in Equation 2.6 (or equivalently Equation 2.9) could reasonably be truncated at first order. Progressing this argument, suppose that two fields were applied to the system, then the leading term detected in all $\boldsymbol{k}_i + \boldsymbol{k}_j$ directions (where $i, j = 1$ or 2) would be dominated by the corresponding second order term of Equation 2.6. This line of reasoning can be extended to describe N_F applied fields, and it very useful for gaining physical insight into an N^{th} order optical spectroscopic process. This is because, within the outlined formalism, the general expression for the system's response to an optical process involving N_F applied fields and detected in a highly specific direction can be found *via* solving for the corresponding N^{th} order density matrix (Equation 2.5). It is upon this foundation that computationally amenable theoretical descriptions of specific optical processes are developed from in later chapters of this manuscript.

Note, as opposed to introducing the density matrix, the many-body wavefunction could be solved in a perturbative nature. However, the density matrix provides a more physically insightful description of the system because populations and intermediate co-

$\mathbf{E}_1(t-\tau_1)e^{\mathbf{k_1}\cdot\mathbf{r}}\mathbf{E}_1(t-\tau_2)e^{i\mathbf{k_1}\cdot\mathbf{r}}$	$\mathbf{k}_s = 2\mathbf{k}_1$	$\omega_s = 2\omega_1$
$\mathbf{E}_1(t-\tau_1)e^{\mathbf{k_1}\cdot\mathbf{r}}\mathbf{E}_1^*(t-\tau_2)e^{-i\mathbf{k_1}\cdot\mathbf{r}}$	$\mathbf{k}_s = 0$	$\omega_s = 0$
$\mathbf{E}_1(t-\tau_1)e^{\mathbf{k_1}\cdot\mathbf{r}}\mathbf{E}_2(t-\tau_2)e^{i\mathbf{k_2}\cdot\mathbf{r}}$	$\mathbf{k}_s = \mathbf{k}_1 + \mathbf{k}_2$	$\omega_s = \omega_1 + \omega_2$
$\mathbf{E}_1(t-\tau_1)e^{\mathbf{k_1}\cdot\mathbf{r}}\mathbf{E}_2^*(t-\tau_2)e^{-i\mathbf{k_2}\cdot\mathbf{r}}$	$\mathbf{k}_s = \mathbf{k}_1 - \mathbf{k}_2$	$\omega_s = \omega_1 - \omega_2$
$\mathbf{E}_1^*(t-\tau_1)e^{-i\mathbf{k_1}\cdot\mathbf{r}}\mathbf{E}_1(t-\tau_2)e^{i\mathbf{k_1}\cdot\mathbf{r}}$	$\mathbf{k}_s = 0$	$\omega_s = 0$
$\mathbf{E}_1^*(t-\tau_1)e^{-i\mathbf{k_1}\cdot\mathbf{r}}\mathbf{E}_1^*(t-\tau_2)e^{-i\mathbf{k_1}\cdot\mathbf{r}}$	$\mathbf{k}_s = -2\mathbf{k}_1$	$\omega_s = -2\omega_1$
$\mathbf{E}_1^*(t-\tau_1)e^{-i\mathbf{k_1}\cdot\mathbf{r}}\mathbf{E}_2(t-\tau_2)e^{i\mathbf{k_2}\cdot\mathbf{r}}$	$\mathbf{k}_s = -\mathbf{k}_1 + \mathbf{k}_2$	$\omega_s = -\omega_1 + \omega_2$
$\mathbf{E}_1^*(t-\tau_1)e^{-i\mathbf{k_1}\cdot\mathbf{r}}\mathbf{E}_2^*(t-\tau_2)e^{-i\mathbf{k_2}\cdot\mathbf{r}}$	$\mathbf{k}_s = -\mathbf{k}_1 - \mathbf{k}_2$	$\omega_s = -\omega_1 - \omega_2$
$\mathbf{E}_2(t-\tau_1)e^{i\mathbf{k_2}\cdot\mathbf{r}}\mathbf{E}_1(t-\tau_2)e^{i\mathbf{k_1}\cdot\mathbf{r}}$	$\mathbf{k}_s = \mathbf{k}_1 + \mathbf{k}_2$	$\omega_s = \omega_1 + \omega_2$
$\mathbf{E}_2(t-\tau_1)e^{i\mathbf{k_2}\cdot\mathbf{r}}\mathbf{E}_1^*(t-\tau_2)e^{-i\mathbf{k_1}\cdot\mathbf{r}}$	$\mathbf{k}_s = -\mathbf{k}_1 + \mathbf{k}_2$	$\omega_s = -\omega_1 + \omega_2$
$\mathbf{E}_2(t-\tau_1)e^{i\mathbf{k_2}\cdot\mathbf{r}}\mathbf{E}_2(t-\tau_2)e^{i\mathbf{k_2}\cdot\mathbf{r}}$	$\mathbf{k}_s = 2\mathbf{k}_2$	$\omega_s = 2\omega_2$
$\mathbf{E}_2(t-\tau_1)e^{i\mathbf{k_2}\cdot\mathbf{r}}\mathbf{E}_2^*(t-\tau_2)e^{-i\mathbf{k_2}\cdot\mathbf{r}}$	$\mathbf{k}_s = 0$	$\omega_s = 0$
$\mathbf{E}_2^*(t-\tau_1)e^{-i\mathbf{k_2}\cdot\mathbf{r}}\mathbf{E}_1(t-\tau_2)e^{i\mathbf{k_1}\cdot\mathbf{r}}$	$\mathbf{k}_s = \mathbf{k}_1 - \mathbf{k}_2$	$\omega_s = \omega_1 - \omega_2$
$\mathbf{E}_2^*(t-\tau_1)e^{-i\mathbf{k_2}\cdot\mathbf{r}}\mathbf{E}_1^*(t-\tau_2)e^{-i\mathbf{k_1}\cdot\mathbf{r}}$	$\mathbf{k}_s = -\mathbf{k}_1 - \mathbf{k}_2$	$\omega_s = -\omega_1 - \omega_2$
$\mathbf{E}_2^*(t-\tau_1)e^{-i\mathbf{k_2}\cdot\mathbf{r}}\mathbf{E}_2(t-\tau_2)e^{i\mathbf{k_2}\cdot\mathbf{r}}$	$\mathbf{k}_s = 0$	$\omega_s = 0$
$\mathbf{E}_2^*(t-\tau_1)e^{-i\mathbf{k_2}\cdot\mathbf{r}}\mathbf{E}_2^*(t-\tau_2)e^{-i\mathbf{k_2}\cdot\mathbf{r}}$	$\mathbf{k}_s = -2\mathbf{k}_2$	$\omega_s = -2\omega_2$

Table 2.1: Column 1 details the sixteen terms resulting from two fields incident on a sample. Columns 2 and 3 give the corresponding signal wave vector, k_s, and signal frequency, ω_s, that a specific optical process is detected at. Notice that some processes have multiple contributions, and a term always has a complex conjugate such that the total polarization is always real.

herences between states become mathematically obvious – whereas only beginning and ending populations are mathematically obvious in the correction to the wavefunction formalism. [5, 34]

2.2 Time Correlation Descriptions & Implementation Considerations

As will be demonstrated in later chapters of this manuscript, the N^{th} order response (susceptibility) a given experiment detects can be expressed in terms of sums and differences of time correlation functions (TCF's). [5,6,35,36] For example, it can be shown [5,37] that the linear response component emitted from a standard FTIR experiment is proportional to the autocorrelation function of the system's dipole operator (Equation 2.13). (Traditional frequency domain spectra, in the limit of monochromatic fields, are obtained *via* Fourier transform of Equation 2.13.)

$$R_{ij}{}^{(1)}(\mathbf{k_s}, t) \propto \frac{i}{\hbar} \int_0^\infty dt' \, \langle \mu^i(0)\mu^j(t')\rangle - \langle \mu^i(t')\mu^j(0)\rangle \tag{2.13}$$

The TCF's in Equation 2.13 are complex quantum mechanical objects – which forces the question: How can these quantities be amenable to classical or semiclassical computation techniques? Before addressing this question, it is instructive to expand the complex TCF's in terms or their real and imaginary parts. Noting that $\langle \mu^i(0)\mu^j(t')\rangle = \{\langle \mu^i(t')\mu^j(0)\rangle\}^*$, and letting $C_I(t)$ [$C_R(t)$] denote the imaginary [real] component of the TCF, Equation 2.13 can analytically be rewritten as:

$$R_{ij}{}^{(1)}(\mathbf{k_s}, t) \propto \frac{2}{\hbar} \int_0^\infty dt' \, C_I(t') \tag{2.14}$$

Further, representing the TCF's in Equation 2.13 in their Heisenberg representation and independently Fourier transforming them, reveals a detailed-balance relationship between the real and imaginary parts: $C_I(\omega) = tanh(\beta\hbar\omega)C_R(\omega)$. [5, 6] Substitution of this relationship into Equation 2.14 and Taylor expansion of the $tanh$ factor reduces the necessary order of $\hbar$, and therefore, establishes a definitive classical limit. (The explicit mathematical derivation of the detailed-balance relationship will be presented in Chapter 3.) In this limit, the system's response becomes proportional to the purely real autocorrelation function of the system's dipole – a quantity that is amenable to standard molecular dynamics (MD) simulation techniques. [6, 17–19, 36, 38, 39]

In principle, it is an achievable goal to incorporate all the necessary potential terms (parametrized with *ab initio* calculations and/or experimental data) in an MD simulation to accurately reproduce the system's electric moments that are required to compute TCF's that correspond to a specific response of a given type of spectroscopy. [40, 41] However, consider, *e.g.*, Equation 2.13 and the McLaurian expansion of the system's dipole operator around position $\mathbf{r}$: $\mu_{ab} = \mu_o\delta_{ab} + \mu'\mathbf{r}_{ab} + \mathcal{O}(r^2)$. The spectroscopic signal a given FTIR experiment measures stems from the perturbing field inducing a transition between states (*i.e.* $a \neq b$). Therefore, $R_{ij}^{(1)}$ in Equation 2.13 must be proportional to the first derivative of the dipole operator. Again, in principle it is possible to accurately capture this quantity using a classical MD potential parametrized with experimental data or *ab initio* calculations when there is a lack of experimental data. [40, 41] However, in practice, it is much more straightforward to use trajectories generated from a classical, comparably

simple, MD potential that models the system's average electric moments accurately, but does not necessarily capture the true value of the derivatives of these quantities. It is very important to note that this type of MD simulation will still capture the true dynamics of the system; the system's electric moment derivatives correspond to infinitesimal changes in an atom's local environment, and therefore do not play any significant role in governing the dynamics of the system. [6,42] It is the electric moment derivatives, however, that provide a window into the complex physics of the system *via* spectroscopy. Herein, we have developed a "spectroscopic model" that uses the trajectories generated from a "simple" MD potential as input, and allows for the system's average electric moments and their derivatives to be calculated for each time step along the trajectory. In the next section, the foundations of the basic spectroscopic model will be outlined.

2.3 A Basic Spectroscopic Model

A spectroscopic model – based upon a Thole-Applequist interaction model [43–46] – has been constructed. The underlying task of the spectroscopic model is to capture how the electrostatic properties of one atom influences the electric moments of another atom, and ultimately how the atoms collectively interact to produce the system's total electrostatic moments. In pursuit of developing this mathematical model, consider a system of a single molecule that is itself composed of several atoms. There is some intrinsic internal field vector, $\mathbf{F}_i$, at each atom "i" due to all the other atom's in the molecule. If an external field is now applied to this molecule, the externally applied field will have a local value of $\mathbf{E}_i^{(o)}$

at atom "i". Further, the presence of the applied field can induce a dipole at each atom "i", and the induced dipole on atom "i" can in turn induce a dipole on atom "j". Now if the total dipole at each atom can be expanded in a McLaurian series around the total electric field, $\mathbf{E}_i^{(tot)}$, it can be written as Equation 2.15. Note, all Roman subscripts denote atoms, and are not to be summed over unless specified. All Greek superscripts denote Cartesian tensor components, and are subject to the Einstein summation convention.

$$\mu_{mol}^{\alpha} = \sum_i \mu_i^{\alpha} = \sum_i \left\{ \mu_i^{(o),\alpha} + \mu'^{\alpha\beta}_i E_i^{(tot),\beta} + \mathcal{O}[(\mathbf{E}_i^{(tot)})^2] \right\} \tag{2.15}$$

Here, $\mu_i^{(o),\alpha}$ is the intrinsic dipole of atom "i" (intrinsic because the expansion is a McLaurian series around the total electric field). Note the second ranked tensor $\mu_i'^{\alpha\beta}$ is generally denoted by $\alpha_i^{\alpha\beta}$, and is the intrinsic polarizability of atom "i". The polarizability of a molecule is a measure of how easily a dipole can be induced. Also notice Equation 2.15 has been truncated at first order. The second and third derivatives of the dipole evaluated at zero total field are often referred to as an atom's intrinsic hyperpolarizability and second hyperpolarizability respectively.

To facilitate mathematical development of the spectroscopic model, the total electric field will be split into its three distinct contributions: $\mathbf{E}_i^{(o)}$+ $\mathbf{F}_i$ + ($\sum_j \mathbf{T}_{ij} \cdot \mu_j = \sum_j \bigtriangledown \bigtriangledown \mathbf{r}_{ij}^{-1} \cdot \mu_j$). The third term corresponds to the field at atom "i" resulting from induced moments on all other atoms. [44, 47]

$$\mu_{mol}^{\alpha} = \sum_i \mu_i^{\alpha} = \sum_i \left\{ \mu_i^{(o),\alpha} + \mu_i'^{\alpha\beta} \left\{ E_i^{(o),\beta} + F_i^{\beta} + \sum_{j \neq i} T_{ij}^{\beta\gamma} \mu_j^{\gamma}] \right\} \right\} \tag{2.16}$$

The derivative of the total dipole evaluated at zero *total* field strength has already been identified as the intrinsic system polarizability. Therefore, it is instructive to write the

partial derivative of Equation 2.16 with respect to the applied field, $\mathbf{E}_i^{(o)}$ because, this can be associated with the system polarizability under the influence of a static electric field.

$$A_{mol}^{\alpha\zeta} = \frac{\partial \mu_{mol}^{\alpha}}{\partial E^{(o),\zeta}} = \sum_i \frac{\partial \mu_i^{\alpha}}{\partial E_k^{(o),\zeta}} = \sum_i \alpha_i^{\alpha\beta} \left\{ \delta_{ik}\delta_{\zeta\beta} + \sum_{j\neq i} T_{ij}^{\beta\gamma} \frac{\partial \mu_j^{\gamma}}{\partial E_k^{(o),\zeta}} \right\} \tag{2.17}$$

$$A_{jk}^{\alpha\zeta} = \frac{\alpha_i^{\alpha\beta}\delta_{jk}\delta_{\zeta\beta}}{\delta_{ij}\delta_{\alpha\gamma} - \alpha_i^{\alpha\beta}\sum_j T_{ij}^{\beta\zeta}} \tag{2.18}$$

Equation 2.18 is a primary result of this section because it provides a mathematical means to calculate the many-body polarizability matrix, A. Further, Equation 2.18 allows the total induced system dipole, $\mu_{mol}^{ind,\alpha}$, to be expressed as:

$$\mu_{mol}^{ind,\alpha} = A_{mol}^{\alpha\zeta}(E^{(o),\zeta} + F^{\zeta}) \tag{2.19}$$

Note, while this present theoretical discussion and mathematical development was conducted under the assumption that the system was composed of a single molecule, this was done for conceptual clarity only. The equations developed in this section, as is, generalize to a system contain any number of molecules.

Translation between this general model developed and our spectroscopic model involves: (1) assuming the atomic polarizability tensors can be approximated as point polarizabilities instead of tensors, $\alpha_i^{\alpha\beta} \longrightarrow \alpha_i \mathbf{I}$, (2) assuming a constant applied field, and (3) introduction of a damping factor to prevent unphysically large induced dipole moments. (1) and (2) are not necessary, and serve only to simply computational efforts. In contrast, (3) is necessary because the system's induced dipole, is a function of inter-nuclear distances, and when an interatomic distance, $\mathbf{r}_{ij}$, approaches $(4\alpha_i\alpha_j)^{1/6}$, unphysically large

values for the induced-dipole moments result. [43] In following chapters, the specifics of how the interaction model is parametrized for a given system will be outlined in detail. Following, for the sake of completeness and clarity, these basic steps will be briefly summarized.

Within the spectroscopic model, any general system is first broken down into the types of molecules that comprise it, and then into the atoms that comprise the specific sets of the different molecular species. Each atom type within a like group of molecular species is assigned a point charge (to reproduce the permenant dipole) and polarizability along with point derivatives. The value of the zeroth and first order terms in the McLaurian expansion for the dipole and polarizability moments (as detailed in the previous section) are chosen such that when the atoms comprising a particular isolated molecular species are allowed to interact, the molecule's electric moments and their derivatives are accurately reproduced. In fitting the model, the zeroth order terms are parametrized first, and are based upon a molecules equilibrium gas phase configuration. The first order terms are subsequently parametrized, and are based upon performing many calculations within our spectroscopic model where small displacements ($\mathcal{O}(E^{-5}\mathring{A})$) from the equilibrium configuration are made such that point difference derivatives can be obtained. Note, the molecule's gas phase electric moments and their derivatives are fit to experimental data and/or *ab initio* calculations.

Chapter 3

Second Order Surface Specific Sum Vibrational Frequency Spectroscopy (SVFS)

The possible second order optical process that occur when a system is perturbed by two impinging electric fields are Sum Harmonic/Sum Frequency/Sum Difference Generation (SFG/SHG/DFG) and optical rectification. Sum vibration frequency spectroscopy (SVFS) is a vibrationally resonant version of SFG, and is a powerful experimental method for probing the structure and dynamics of interfaces. SVFS experiments typically employ two fields, a visible (vis) and an infrared (IR), overlapped in time and space at an interface. In most cases, the frequency of the visible field is fixed, and the IR frequency range is scanned. The signal SVFS measures is proportional to the second order polarization component in the sum wave vector direction and at the sum frequency of applied perturbing fields: $\mathbf{P}^{(2)}(\mathbf{k_s} = \mathbf{k}_{vis}+\mathbf{k}_{IR}, \omega_s = \omega_{vis}+\omega_{IR})$. In the absence of any vibrational resonance at the instantaneous IR laser frequency, a structureless signal due to the static hyperpolarizability of the interface is obtained. [48–50] When the IR laser frequency is in tune with a vibration at the interface, a resonant lineshape having a characteristic shape that reflects both the structural and dynamical environment at the interface, is produced. [51–53]

SVFS, as well as all even ordered polarization measurements, are interface specific in the dipole approximation due to symmetry constraints. This can be understood by considering an isotropic system with any number of fields applied to it. If the direction of all the electric fields in an experiment were reversed, the sign of The polarization must change because all directions are equivalent on average. [2] However, even numbers of applied fields will make the polarization equal to its negative – a condition that insists the polarization is zero, *i.e.* $\mathbf{P} = -\mathbf{P} = 0$. [5] At an interface, or in certain noncentrosymmetric solids, [3] the isotropy of the system is broken. This leads to a second order signal within the dipole approximation, and in this case, the signal is proportional to the product of the susceptibility and the electric fields as described by Equation 2.10.

Recent years have seen a great increase in the number of experimental groups performing SVFS investigations. [7, 12, 54–61] In contrast, molecularly detailed theoretical simulations of SVFS spectra are comparatively few, and have only recently begun making a significant impact. Like all vibrational spectroscopies, the goal of SVFS is to infer structural and dynamical properties from the observed spectroscopic signatures. In contrast to more traditional vibrational spectroscopies, SVFS lineshapes tend to be more complex (reflecting the unique environment that is present at an interfacial boundary), and are not nearly as well understood. Thus, the advent of effective theoretical simulation techniques promises to help realize the potential of SVFS to permit detailed characterization of interfaces on par with that done in the bulk. To this end, a TCF theory of SVFS, based upon the density matrix formalism outlined in Chapter 2, and amenable to semiclassical com-

putational techniques was developed. Following, the construction of this theory will be outlined and discussed. Subsequently, its practical application to a liquid water interface will be presented.

3.1 Theoretical Development of the Governing SVFS TCF

Formally a second order polarization, the dominant $\mathbf{r}$ space contribution in a typical SVFS experiment is given by:

$$\mathbf{P}^{(2)}(\mathbf{r}, \omega_{IR}, \omega_{vis}) = \langle \rho^{(2)} \boldsymbol{\mu} \rangle = 2\pi \sum_{\mathbf{k_s}} e^{i(\mathbf{k_s})\cdot\mathbf{r}} \boldsymbol{\chi}^{(2)}(\omega_{IR}, \omega_{vis}) : \mathbf{E}_1 \mathbf{E}_2 \tag{3.1}$$

Equation 3.1 assumes the dipole approximation. Therefore, the perturbing Hamiltonian operator is defined as: $H^{(1)}(t) = -\boldsymbol{\mu}\cdot\mathbf{E}(t)$. From a theoretical standpoint, the primary quantity of interest is the system's susceptibility tensor, $\boldsymbol{\chi}$, because whereas the fields are input variables, the susceptibility is an intrinsic property of the system, and contains all the information that can be probed. [2–6] A microscopic expression for $\boldsymbol{\chi}^{(2)}$ can be developed by solving for the second order density matrix, and equating the latter two equalities in Equation 3.1.

Given the perturbative approach outlined in Chapter 2, the solution to the second order density matrix can be seen to be a function of the first order density matrix, and the solution to the first order density matrix can be seen to be a function of the zeroth order density matrix. The zeroth order density matrix is known, and is given by a standard Boltzmann distribution: $\rho^{(0)} = \rho_{eq} = \frac{e^{-\beta H}}{Q}$, where Q is the partition function and β is the

reciprocal of Boltzmann's constant multiplied by temperature. The solution for $\rho^{(1)}$ under the stated conditions will be found first.

$$\rho^{(1)}_{nm}(t) = \left(\frac{-i}{\hbar}\right) e^{-it(\omega_{nm}-i\gamma_{nm})} \int_{-\infty}^{t} dt' \, [H^{(1)}(t'), \rho^{(0)}]_{nm} \, e^{it'(\omega_{nm}-i\gamma_{nm})} \tag{3.2}$$

Isolating the commutator in Equation 3.2, and projecting with a complete set of states, v, results in:

$$[H^{(1)}(t), \rho^{(0)}]_{nm} = \sum_{v} \left\{-\boldsymbol{\mu}_{nv}\rho^{(0)}_{vm} \cdot \boldsymbol{E}(\mathrm{t}) + \rho^{(0)}_{nv}\boldsymbol{\mu}_{vm} \cdot \boldsymbol{E}(\mathrm{t})\right\} \tag{3.3}$$

As discussed in Chapter 2, the zeroth order density matrix is assumed to be diagonal. This approximation allows Equation 3.3 to be written as Equation 3.4, and this representation of the commutator can be substituted back into Equation 3.2 to give Equation 3.5.

$$[H^{(1)}(t), \rho^{(0)}]_{nm} = (\rho^{(0)}_{nn}\boldsymbol{\mu}_{nm} - \boldsymbol{\mu}_{nm}\rho^{(0)}_{mm}) \cdot \boldsymbol{E}(\mathrm{t}) \tag{3.4}$$

$$\rho^{(1)}_{nm}(t) = \frac{i}{\hbar} e^{-it(\omega_{nm}-i\gamma_{nm})}(\rho^{(0)}_{mm} - \rho^{(0)}_{mm})\boldsymbol{\mu}_{nm} \cdot \sum_{p} \boldsymbol{E}(\omega_p) \int_{-\infty}^{t} dt' e^{-it(\omega_p - \omega_{nm} + i\gamma_{nm})} \tag{3.5}$$

Note in Equation 3.5, the applied field has been represented in terms of a Fourier series, and ω_p is a completely general frequency at this point. Analytic ($\int_{-\infty}^{t} dt' \; e^{it'(a-ib)} = \frac{i}{a-ib} \; e^{it(a-ib)}$) integration of Equation 3.5 yields:

$$\rho^{(1)}_{nm}(t) = \frac{1}{\hbar}(\rho^{(0)}_{mm} - \rho^{(0)}_{nn}) \sum_{p} e^{-it\omega_p} \left[\frac{\boldsymbol{\mu}_{nm} \cdot \boldsymbol{E}(\omega_p)}{\omega_{nm} - \omega_p - i\gamma_{nm}}\right] \tag{3.6}$$

Equation 3.6 is the perturbative solution to the first order power series expansion of the density matrix equation of motion. It is from this term that an expression for the linear

susceptibility, $\chi^{(1)}$, can be determined, and it is also the starting point for solving for the second order density matrix. We proceed by solving for $\rho^{(2)}$.

$$\rho_{nm}^{(2)}(t) = \left(\frac{-i}{\hbar}\right) e^{-it(\omega_{nm}-i\gamma_{nm})} \int_{-\infty}^{t} dt' \, [H^{(1)}(t'), \rho^{(1)}(t)]_{nm} e^{it'(\omega_{nm}-i\gamma_{nm})} \tag{3.7}$$

Expanding the commutator, and representing the second applied field in terms of a Fourier series that is a function of a general ω_q gives:

$$\begin{aligned}
&[H^{(1)}(t), \rho^{(1)}(t)]_{nm} = \sum_{v} [\rho_{nv}^{(1)} \boldsymbol{\mu}_{vm} - \boldsymbol{\mu}_{nv} \rho_{vm}^{(1)}] \cdot \boldsymbol{E}(\mathrm{t}) \\
&= \frac{1}{\hbar} \sum_{vpq} \frac{\rho_{nn}^{(0)} - \rho_{vv}^{(0)}}{\omega_p - \omega_{nv} + i\gamma_{nv}} \left\{ [\boldsymbol{\mu}_{nv} \cdot \boldsymbol{E}(\omega_q)][\boldsymbol{\mu}_{vm} \cdot \boldsymbol{E}(\omega_q))] e^{-it(\omega_p+\omega_q)} \right\} \\
&- \frac{1}{\hbar} \sum_{vpq} \frac{\rho_{vv}^{(0)} - \rho_{mm}^{(0)}}{\omega_p - \omega_{vm} + i\gamma_{vm}} \left\{ [\boldsymbol{\mu}_{vm} \cdot \boldsymbol{E}(\omega_p)][\boldsymbol{\mu}_{nv} \cdot \boldsymbol{E}(\omega_q)] e^{-it(\omega_p+\omega_q)} \right\}
\end{aligned} \tag{3.8}$$

Inserting the expanded commutator in Equation 3.8 into Equation 3.7, and subsequently performing the necessary integration yields:

$$\begin{aligned}
\rho_{nm}^{(2)}(t) = \frac{1}{\hbar^2} \sum_{vpq} \Bigg[&\frac{e^{-it(\omega_p+\omega_q)} (\rho_{nn}^{(0)} - \rho_{vv}^{(0)}) [\boldsymbol{\mu}_{nv} \cdot \boldsymbol{E}(\omega_p)][\boldsymbol{\mu}_{vm} \cdot \boldsymbol{E}(\omega_q)]}{(\omega_p - \omega_{nv} + i\gamma_{nv})(\omega_p + \omega_q - \omega_{nm} + i\gamma_{nm})} \\
&- \frac{e^{-it(\omega_p+\omega_q)} (\rho_{vv}^{(0)} - \rho_{mm}^{(0)}) [\boldsymbol{\mu}_{vm} \cdot \boldsymbol{E}(\omega_p)][\boldsymbol{\mu}_{nv} \cdot \boldsymbol{E}(\omega_q)]}{(\omega_p - \omega_{vm} + i\gamma_{vm})(\omega_p + \omega_q - \omega_{nm} + i\gamma_{nm})} \Bigg]
\end{aligned} \tag{3.9}$$

Making a change of dummy indices in Equation 3.9 and substituting into Equation 3.1 produces a dipolar general expression for the second order susceptibility. Building in intrinsic permutation symmetry [2] to the second order susceptibility, and now specify that $\omega_p = \omega_{vis}$, $\omega_q = \omega_{IR}$, and $\omega_{IR} + \omega_{vis} = \omega_s$ results in an expression for $\boldsymbol{\chi}^{(2)}$ that is a sum of eight terms. These eight terms are detailed below. Note, Equation 3.10 expresses

the total second order susceptibility, a third ranked tensor, in terms of its Cartesian tensor components.

$$\begin{aligned}\boldsymbol{\chi}^{(2)}_{ijk} = \frac{M}{\hbar^2}\sum_{mng}\rho^{(0)}_{gg}\Bigg[&\frac{\mu^i_{gn}\mu^j_{nm}\mu^k_{mg}}{(\omega_s-\omega_{ng}+i\gamma_{ng})(\omega_{IR}-\omega_{mg}+i\gamma_{mg})}\\ &-\frac{\mu^j_{gn}\mu^i_{nm}\mu^k_{mg}}{(\omega_{vis}+\omega_{ng}+i\gamma_{ng})(\omega_{IR}-\omega_{mg}+i\gamma_{mg})}\\ &+\frac{\mu^k_{gn}\mu^j_{nm}\mu^i_{mg}}{(\omega_s+\omega_{mg}+i\gamma_{mg})(\omega_{IR}+\omega_{ng}+i\gamma_{ng})}\\ &-\frac{\mu^k_{gn}\mu^i_{nm}\mu^j_{mg}}{(\omega_{vis}-\omega_{mg}+i\gamma_{mg})(\omega_{IR}+\omega_{ng}+i\gamma_{ng})}\\ &+\frac{\mu^j_{gn}\mu^i_{mg}\mu^k_{nm}}{(\omega_s+\omega_{mg}+i\gamma_{mg})(\omega_{vis}+\omega_{ng}+i\gamma_{ng})}\\ &+\frac{\mu^i_{gn}\mu^j_{mg}\mu^k_{nm}}{(\omega_s-\omega_{ng}+i\gamma_{ng})(\omega_{vis}-\omega_{mg}+i\gamma_{mg})}\Bigg]\end{aligned} \tag{3.10}$$

Formally, the susceptibility detailed in Equation 3.10 is a quantum mechanical object that appears to not have a well defined classical limit ($\hbar \longrightarrow 0$). To develop a theory that is amenable to classical or semiclassical computation techniques, a distinct classical limit of this expression must be obtainable. This limit is more than just book keeping; it establishes a definitive quantum-classical correspondence, and validates that a method using classical or semiclassical computational techniques can capture the true physics of the optical process.

In pursuit of establishing a well defined classical limit of $\boldsymbol{\chi}^{(2)}_{ijk}$, the dimensionality of $\hbar$ must be reduced. To accomplish this, the nature of the applied fields that are characteristic of an SVFS experiment are considered. As noted previously, only the infrared field is vibrationally resonant – both the sum frequency and visible fields fall far from resonance, and typical SVFS experiments are also electronically nonresonant. With these

considerations in mind, terms in Equation 3.10 that will dominate when the frequency of the infrared field becomes vibrationally resonant with a mode in noncentrosymmetric media can be identified. This observation facilitates writing $\boldsymbol{\chi}^{(2)}$ in terms of a resonant ($\boldsymbol{\chi}_{ijk}^{(2)RES}$) and nonresonant ($\boldsymbol{\chi}_{ijk}^{(2)NR}$) contribution.

$$\boldsymbol{\chi}_{ijk}^{(2)} = \boldsymbol{\chi}_{ijk}^{(2)RES} + \boldsymbol{\chi}_{ijk}^{(2)NR} \tag{3.11}$$

$$\boldsymbol{\chi}_{ijk}^{(2)RES} = \sum_{mng} \frac{\rho_{gg}^{(0)}}{\hbar^2} \left[\left(\frac{\mu_{mg}^{k}}{(\omega_{IR} - \omega_{mg} + i\gamma_{mg})} \right) * \right.$$

$$\left(\frac{\mu_{gn}^{i}\mu_{nm}^{j}}{(\omega_s - \omega_{ng} + i\gamma_{ng})} - \frac{\mu_{gn}^{j}\mu_{nm}^{i}}{(\omega_{vis} + \omega_{ng} + i\gamma_{ng})} \right.$$

$$\left. \left. + \left(\frac{\mu_{nm}^{j}\mu_{mg}^{i}}{(\omega_s + \omega_{mg} + i\gamma_{mg})} - \frac{\mu_{nm}^{i}\mu_{mg}^{j}}{(\omega_{vis} - \omega_{mg} + i\gamma_{mg})} \right) \left(\frac{\mu_{gn}^{k}}{(\omega_{IR} + \omega_{ng} + i\gamma_{ng})} \right) \right] \tag{3.12}$$

$$\boldsymbol{\chi}_{ijk}^{(2)NR} = \sum_{mng} \frac{\rho_{gg}^{(0)}}{\hbar^2} \left[\frac{\mu_{gn}^{j}\mu_{mg}^{i}\mu_{nm}^{k}}{(\omega_s + \omega_{mg} + i\gamma_{mg})(\omega_{vis} + \omega_{ng} + i\gamma_{ng})} \right.$$

$$\left. + \frac{\mu_{gn}^{i}\mu_{mg}^{j}\mu_{nm}^{k}}{(\omega_s - \omega_{ng} + i\gamma_{ng})(\omega_{vis} - \omega_{mg} + i\gamma_{mg})} \right] \tag{3.13}$$

From here on, focus will be only on $\boldsymbol{\chi}_{ijk}^{(2)RES}$ because it provides the most information pertaining to the resonant vibrational lineshape. Because both the signal and visible fields fall far from resonance, it is approximated that $1/\omega_s \approx 1/\omega_{vis}$. This approximation allows for the $\hbar$ dimensionality of $\boldsymbol{\chi}_{ijk}^{(2)RES}$ to be reduce by one order through the introduction of the system polarizability operator. The system polarizability operator is essentially the first order susceptibility, and is defined as:

$$\alpha^{ij}(\omega) = \frac{1}{\hbar} \sum_{g,n} \left[\frac{\mu_{gn}^{i}\mu_{ng}^{k}}{-\omega + \omega_{ng} - i\gamma_{ng}} + \frac{\mu_{gn}^{k}\mu_{ng}^{i}}{\omega + \omega_{ng} + i\gamma_{ng}} \right] \tag{3.14}$$

Utilizing Equation 4.13, the resonant second order susceptibility can be written as a sum of two terms.

$$\boldsymbol{\chi}_{ijk}^{(2)RES} = -\frac{1}{\hbar}\sum_{mg}\rho_{gg}^{(0)}\left(\frac{\alpha_{gm}^{pq}\mu_{mg}^{k}}{(\omega_{IR}-\omega_{mg}+i\gamma_{mg})}\ \frac{\mu_{gn}^{k}\alpha_{ng}^{pq}}{(\omega_{IR}+\omega_{ng}+i\gamma_{ng})}\right) \tag{3.15}$$

The resonant denominators in Equation 3.15 can each be replaced using integral identities: $\int_0^\infty dt\ e^{-it(\omega-\omega_o-i\gamma)} = \frac{-i}{\omega-\omega_o-i\gamma}$ and $\int_0^\infty dt\ e^{it(\omega+\omega_o+i\gamma)} = \frac{i}{\omega+\omega_o+i\gamma}$. Because γ is a phenomenological damping factor that is naturally incorporated into the dynamics of the system, the implied limit that gamma goes to zero is also taken. Performing these steps allows Equation 3.15 to be written as:

$$\chi_{ijk}^{Res} = \frac{i}{\hbar}\int_0^\infty\left[\sum_{gm}e^{-i\omega_{mg}t}e^{i\omega_{IR}t}\alpha_{gm}^{ij}\mu_{mg}^{k}\,dt - \sum_{ng}e^{i\omega_{ng}t}e^{i\omega_{IR}t}\alpha_{ng}^{ij}\mu_{gn}^{k}\,dt\right]\rho_{gg}^{(0)} \tag{3.16}$$

$$\chi_{ijk}^{Res} = \frac{i}{\hbar}\int_0^\infty dt\ e^{it\omega_{IR}} < \alpha^{ij}(t)\mu^{k}(0) > - \int_0^\infty dt\ e^{it\omega_{IR}} < \mu^{k}(0)\alpha^{ij}(t) > \tag{3.17}$$

Equation 3.17 follows as an exact rewrite of Equation 3.16, and expresses the SVFS resonant second order susceptibility in terms of the cross correlation of the system dipole and polarizability operators. Note, in deriving Equation 3.17 from 3.16, the Heisenberg representation of the time dependent system polarizability operator, $\alpha^{ij}(t)$, was used, and a sum over states was performed to remove a resolution of the identity. [24, 37]

Further simplification of Equation 3.17 is possible because the two TCF's it is comprised of are complex conjugates – $< \mu^{k}(0)\alpha^{ij}(t) >= C_R(t) + iC_I(t) = (< \alpha^{ij}(t)\mu^{k}(0) >)^*$. [37] Expressing the TCF's in Equation 3.17 explicitly as the sum or difference of their

real, $C_R(t)$, and imaginary, $C_I(t)$, components equates the resonant SVFS susceptibility with an exponential integral over the imaginary component of the correlation function.

$$\chi_{ijk}^{Res}(\omega_{IR}) = \frac{2}{\hbar}\int_0^\infty dt\; e^{it\omega_{IR}}\; C_I(t) \tag{3.18}$$

Equation 3.18 presents χ_{ijk}^{Res} as an explicit function of the IR frequency because the other off-resonant optical frequencies, ω_{vis} and ω_s, have been implicitly absorbed into the polarizability. Equation 3.18 is a nearly exact rewrite (exact other than substituting $1/\omega_s \approx 1/\omega_{vis}$) of the perturbation expression, but there is still one order of $\hbar$ that must be eliminated to establish a well defined classical limit of the resonant SVFS second order susceptibility. To accomplish this, the TCF's in Equation 3.17 will be considered in their corresponding frequency space representation. Note, C_I is odd in frequency and time, and C_R is even in frequency and time. [37, 62, 63] Thus, while $C(t)$ is complex, $C(\omega)$ is purely real.

$$C(\omega) = \sum_{gn}\int_{-\infty}^{\infty} dt\; e^{i\omega t}\rho_g\alpha_{gn}\mu_{ng}e^{-i\omega_{ng}t} = \frac{1}{Q}\sum_{gn} e^{-\beta\hbar\omega_g}\alpha_{gn}\mu_{ng}\delta(\omega-\omega_{ng}) \tag{3.19}$$

$$C^*(\omega) = \sum_{gn}\int_{-\infty}^{\infty} dt\; e^{i\omega t}\rho_g\mu_{gn}\alpha_{ng}e^{i\omega_{ng}t} = \frac{1}{Q}\sum_{gn} e^{-\beta\hbar\omega_g}\mu_{gn}\alpha_{ng}\delta(\omega+\omega_{ng}) \tag{3.20}$$

Letting $n \leftrightarrow g$:

$$C^*(\omega) = \frac{1}{Q}\sum_{gn} e^{-\beta\hbar\omega_n}\alpha_{gn}\mu_{ng}\delta(\omega-\omega_{ng}) \tag{3.21}$$

Equation 3.21 differs from Equation 3.19 only in the Boltzmann factor, and if the delta function is enforced, a detailed balance relationship between $C(\omega)$ and $C^*(\omega)$ can be identified.

$$C(\omega) = e^{\beta\hbar\omega} C^*(\omega) \tag{3.22}$$

Proceeding with some additional algebra:

$$C(\omega) = C_R(\omega) + C_I(\omega) = e^{\beta\hbar\omega} \left(C_R(\omega) - C_I(\omega)\right) \tag{3.23}$$

$$C_R(\omega) \left(e^{\beta\hbar\omega} - 1\right) = \left(1 + e^{\beta\hbar\omega}\right) C_I(\omega) \tag{3.24}$$

$$C_I(\omega) = tanh\left(\frac{\beta\hbar\omega}{2}\right) C_R(\omega) \tag{3.25}$$

The relationship detailed by Equation 3.25 between the real and imaginary parts of the correlation function addresses two physical constraints of the problem. First, how does one calculate the imaginary component of a TCF using classical MD? This relationship equates the only quantity that can be computed using classical MD, $C_R(t)$, and the formal object that describes the spectroscopy, $C_I(t)$. Secondly, a definitive classical limit of the susceptibility must be obtainable if the true physics of the optical process can be captured using classical or semiclassical computation techniques. In the limit $\hbar$ tends toward zero, $tanh\left(\frac{\beta\hbar\omega}{2}\right) \longrightarrow \frac{\beta\hbar\omega}{2}$. Thus, all orders of $\hbar$ cancel, and a well defined classical limit is obtained. Equation 3.26 summarizes the final relationship, and is the principle result of this section.

$$\chi_{ijk}^{Res}(\omega_{IR}) = \frac{2}{\hbar} \int_0^\infty dt\, e^{it\omega_{IR}}\, tanh\left(\frac{\beta\hbar\omega}{2}\right) C_R(t) \longrightarrow \beta\omega \int_0^\infty dt\, e^{it\omega_{IR}} C_R(t) \tag{3.26}$$

Before concluding this section, and discussing the application of the theory developed herein, it should be highlighted that the relationship detailed by Equation 3.25 is completely general. It is valid for any two-point, one-time, correlation function. However, note that because the sign of the forward and reverse Fourier transfers often differ from one text to the next (despite there being a formally correct quantum mechanical sign requirement), sometimes there is a minus sign associated with this $tanh$ detailed balance relationship – as long as all forward and reverse Fourier transforms are consistent within this type of (cyclical) derivation, both conventions will produce the same answer.

3.2 SVFS – Application of Theory & Computational Methods

In order to calculate the time dependent spectroscopic observables inherent in the usual SVFS TCF, a spectroscopic model that supplements the MD force fields must be established. The foundations of our basic spectroscopic model (BSM) have been presented in Chapter 2. Briefly, the permanent dipole, polarizability, and their derivatives for each species present in an MD simulation is parametrized as a function of molecular geometry *via* detailed electronic structure (ES) calculations or experiment. To account for induced dipoles and polarizabilities arising from interatomic interactions, a point atomic polarizability model of the Thole-Applequist interaction model (referred to here as PAPA) type is used. [6, 18, 19, 34, 43, 44] The PAPA model's accuracy arises from its natural incorporation of the intrinsic dipole and polarizability parameters and the explicit incorporation of condensed phase interactions between the polarizable sites.

Previous studies [6, 18, 19, 38, 64, 65], have validated the effectiveness of using this semiclassical computation technique (classical MD + BSM) to calculate the spectroscopic signatures of complex liquids and interfaces. In the context of SVFS, many of these previous studies have focused on interfacial water, and have allowed for substantial new physical insight into this system to be realized. For example, a novel vibrational mode around 875 cm^{-1} present exclusively at the water/vapor interface was discovered. [6, 19] Other recent experiments [66, 67] and theory [68] have indirectly inferred the presence of this novel surface species – a water molecule with two dangling hydrogens. The reason experimental studies have only been able to infer the existence of this species is purely due to technological barriers – there is a lack of intense tunable IR radiation sources in the lower frequency range. [69–71]

Studies using classical MD supplemented with the BSM are capable of not only accurately capturing a system's interfacial or bulk resonant lineshape but the physically significant fine details within this lineshape. Specifically, in context of SVFS, distinct subpopulations that occur at a water/vapor interface and collectively contribute to the OH stretching spectral region have been identified. [6, 19] This was accomplished *via* exploiting the absorptive and dispersive nature of the calculated real and imaginary components of the resonant SVFS susceptibility. The frequencies of the identified subspecies compare exceptionally well with those observed by two separate experimental groups. [48, 72, 73] The average deviation between the theoretical and experimental determinations was less than 1%. [6, 19]

Collectively, the data presented evidences the robustness of the BSM, and its ability to capture the complex many-body interactions present in a condensed phase system. (In neat liquid water nonetheless!) However, in fitting the point electric moments and electric moment derivatives for a given isolated gas phase molecule, there is not necessarily a unique solution. This is the case with water. Several solutions have been found for water that appear to reproduce both the infrared, Raman, and SVFS homodyne detected spectra. However, very recent experimental work [73] was thought to have revealed an incorrect change of phase in our past calculation of the real and imaginary components of the susceptibility for the water/vapor interface in the OH stretching region. All phase information outside of the OH stretching region matched experimentally obtained spectra. This previously went unnoticed because, due to technological barriers; only the square modulus of the SVFS signal was able to be experimentally obtained. Given that our semiclassical computation techniques are able to reproduce such fine detail as the location of subpopulations of vibrational species, the phase error was thought to be due to choosing the wrong solution obtained from fitting the point polarizability and polarizability derivatives. Thus, this motivated refitting the BSM for water based upon ES calculations of an isolated water molecule.

All ES calculations were done using PCGAMESS at the aug-cc-pvqz basis set level, and electron correlation was accounted for using MP2. The polarizability tensor was calculated using ES, and these values were used to parametrize our water model. [6, 19, 74] Specifically, an algorithm was implemented to solve for the point polarizabilities of Oxy-

ES	x	y	z
O	0.	0.	-0.065565653769
H1	0.7569498491	0.	0.5202848504
H2	-0.7569498491	0.	0.5202848504
rOH	0.957180		

Table 3.1: The equilibrium configuration of an isolated water molecule used in ES calculations. Units are in Angstroms.

gen and Hydrogen such that when the electric moments were allowed to interact *via* the BSM, the polarizability tensor obtained from the ES calculation was reproduced. Tables 3.1 and 3.2 detail the water configuration used in the ES and BSM calculations respectively. Note, the configurations between ES and BSM vary. This is because the BSM uses the equilibrium configuration of the MD model, whereas the ES configuration is obtained from experiment. It was found that several solutions were capable of reproducing the polarizability tensor. These solutions were then further tested by assessing their capability to reproduce the polarizability derivative matrix. Constructing the polarizability derivative matrix using our spectroscopic model involved making 9 independent calculations. In each calculation, a single coordinate was displaced by 0.00001Å (in the x, y, or z directions of the Oxygen and 2 Hydrogens) from the equilibrium configuration of water. The set of point polarizabilities (Oxygen=1.307 $\text{Å}^3/e$, Hydrogen=0.157$\text{Å}^3/e$) that naturally best captured the derivative matrix as defined by the ES calculations was

BSM	x	y	z
O.	0.	0.	0.
H1	0.8179551669	0.	0.5752961881
H2	-0.8179551669	0.	0.5752961881
rOH	1.0		

Table 3.2: The equilibrium configuration of an isolated water molecule used in the basic spectroscopic model (BSM) calculations. Units are in Angstroms.

ES	x	y	z	BSM	x	y	z
x	1.512355	0.	0.	x	1.562470	0.	0.
y	0.	1.441227	0.	y	0.	1.31758	0.
z	0.	0.	1.469676	z	0.	0.	1.424445
$\langle\alpha\rangle$	1.47442			$\langle\alpha\rangle$	1.434832		

Table 3.3: The polarizability tensor ($\text{Å}^3/e$) of an isolated water molecule calculated *via* ES and BSM.

α_{ij}	xx	yy	zz	xz=zx	xy=yx	yz=zx
Ox:ES	–	–	–	1.080	–	–
Ox:BSM	–	–	–	1.080	–	–
%Error	–	–	–	0.	–	–
Oz:ES	-1.479	-0.463	-1.282	–	–	–
Oz:BSM	-1.508	-0.475	-1.254	–	–	–
%Error	1.961	2.592	-2.184	–	–	–
H1x:ES	1.281	0.401	0.672	–	–	0.543
H1x:BSM	1.345	0.339	0.635	–	–	0.540
%Error	5.00	15.461	5.82	–	–	0.552
H1z:ES	0.691	0.230	0.575	–	–	0.420
H1z:BSM	.754	0.238	0.627	–	–	0.464
%Error	9.117	3.478	-8.293	–	–	10.476
H2x:ES	-1.388	-0.405	-0.803	–	–	-0.543
H2x:BSM	-1.345	-0.339	-0.635	–	–	-0.540
%Error	3.098	16.296	20.922	–	–	-0.552
H2z:ES	0.691	0.230	0.575	–	–	0.420
H2z:BSM	0.754	0.238	0.627	–	–	0.464
%Error	9.117	3.478	9.043	–	–	10.476

Table 3.4: Polarizability derivative matrix. ES and BSM are compared for the 9 coordinate displacements. Only derivatives with an order of magnitude ≥ 0.1 Å$^2/e$ are presented.

selected to be further refined. Table 3.3 details the polarizability matrix the selected set of point polarizabilities produced, and compares them with ES polarizability values. To the selected set of point polarizabilities, point polarizability derivatives were fit as a function of displacement from equilibrium bond length: $\alpha = \alpha_o + \alpha' \Delta r$. The parameters determined for the point polarizability derivatives were Oxygen=.353 $\text{Å}^2/e$ and Hydrogen=.885 $\text{Å}^2/e$. Table 3.4 gives the derivative polarizability tensor obtained from both the BSM and ES calculations along with the percent error of the BSM polarizability derivative matrix. Note, the polarizability derivative matrix obtained *via ab initio* calculations used the same coordinate displacement method detailed previously.

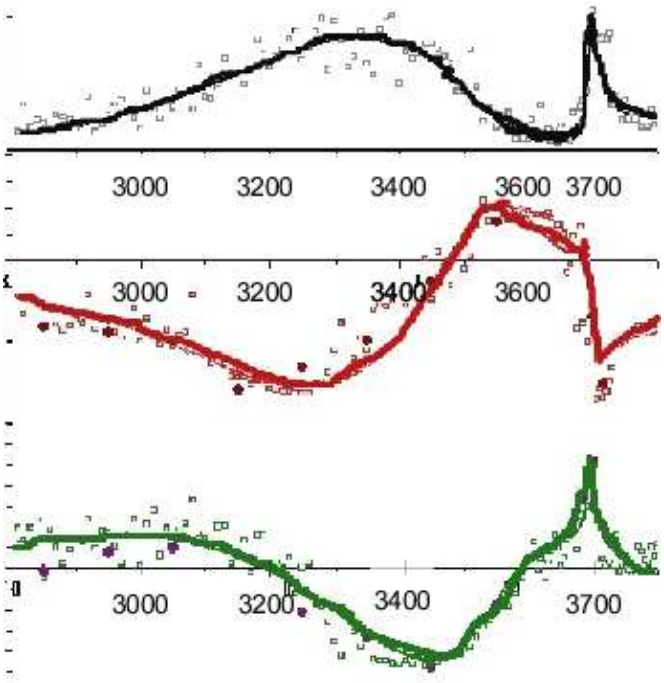

Figure 3.1: Experimental SVFS results for the water/vapor interface. Top Panel: Resonant homodyne signal. Middle Panel: Real component of the resonant signal. Bottom Panel: Imaginary contribution to the resonant signal. In all cases the x-axis is in wavenumbers, and the y-axis is in arbitrary units.

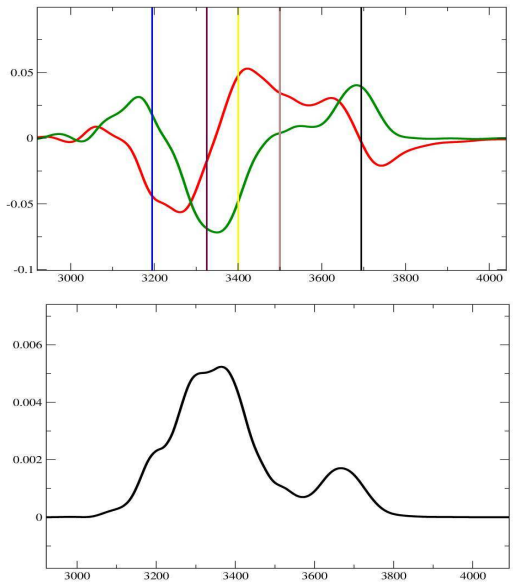

Figure 3.2: Calculated spectra of the water/vapor interface using the reparametrized spectroscopic model. Top Panel: Comparison of the real (red) and imaginary (green) components of the SVFS resonant signal. The lines represent the experimentally obtained locations of subpopulations: 3195 cm^{-1} (blue), 3325 cm^{-1} (purple), 3400 cm^{-1} (yellow), 3500 cm^{-1} (tan), 3694 cm^{-1} (black). In the calculated spectra, a subpopulation is identified by having one of the lineshapes express an absorptive characteristic and the other possess a dispersive characteristic in the same spectral range. Bottom Panel: Calculated resonant homodyne signal.

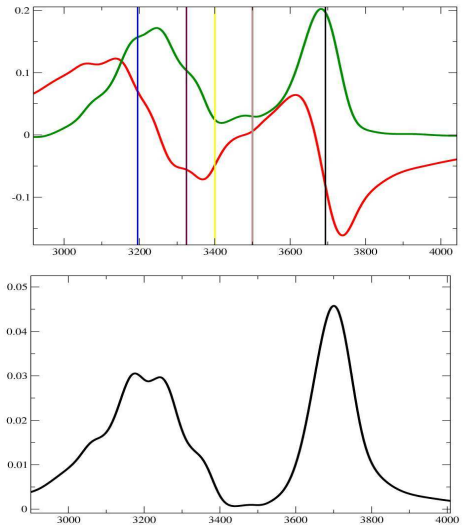

Figure 3.3: Calculated spectra of the water/vapor interface using the old spectroscopic model. Top Panel: Comparison of the real (red) and imaginary (green) components of the SVFS resonant signal. The lines represent the experimentally obtained locations of subpopulations: 3195 cm^{-1} (blue), 3325 cm^{-1} (purple), 3400 cm^{-1} (yellow), 3500 cm^{-1} (tan), 3694 cm^{-1} (black). In the calculated spectra, a subpopulation is identified by having one of the lineshapes express an absorptive characteristic and the other possess a dispersive characteristic in the same spectral range. Bottom Panel: Calculated resonant homodyne signal.

Figures 3.1 – 3.3 show the lineshapes obtained from the new model, the old model, and the latest experimental data collected by the Shen group. [73] The real and imaginary spectra calculated *via* the new model appear to be in much better agreement with the experimentally obtained real and imaginary lineshapes. However, the intensity of the calculated homodyne (square modulus) signal is not correct for the new model, and is better captured by the previous model. This discrepancy can be explained.

In the old water model, the polarizability derivatives where chosen based upon their ability to produce the most intense free OH stretching peak when calculating the homodyne SVFS water/vapor interface spectrum. (Due to technological limitations, this was previously the only quantity that could be measured experimentally.) The new polarizability derivative parameters were chosen because of their ability to accurately reproduce the gas phase water polarizability derivative tensor. Because the intensity of a lineshape is inherently tied to quantum mechanical phenomenon, the new model, while semiclassical in nature and also employing a quantum correction technique, must not be capturing the true population of states. The old model was unphysically adjusted to do so in the OH stretching region, but making this unphysical adjustment in the old model affected other portions of the lineshape also. Namely, this is why the peak around 3400 cm^{-1} lacks intensity in the spectrum produced *via* implementation of the old model. It is important to note, that while not capturing all the quantum mechanical physics of the system, our semiclassical method is quite robust as evidenced by its ability to reproduce the correct many-body interactions in liquid water that result in a sizable shift in fundamental res-

onant vibrational frequency in the condensed phase as compared to the gas phase. (The spectroscopic model was fit to an isolated water molecule.) Secondly, one must be mindful when comparing the intensity of calculated and experimentally obtained lineshapes. This is because the intensity of the experimentally obtained SVFS homodyne spectra is strongly influenced (roughly proportional to the square of the frequency a resonant peak appears at) by necessary experimental parameters, and there is no general convention for removing these effects from the detected signal. [3, 4, 6, 75] When decomposed into the real and imaginary spectra, the error in intensity reduces to roughly order ω. Due to a distinct combination of the two phenomenon discussed, this is why the real and imaginary spectra calculated with the new model are in good agreement with experimental data, and the square modulus signal possesses the correct lineshape but incorrect relative intensity.

Neglecting the intensity differences, Figures 3.1 – 3.3 are all in agreement with respect to subpopulation location and phase. What about the apparent phase error that motivated the complete reparametrization of a new spectroscopic model for water? It was found that the apparent phase error was a result of a restraining potential used in the MD calculations to prevent a water molecule starting in one half of the simulation box from diffusing to the other side's interface – which would result in signal cancellation. [6, 19] Thus, if the restraining potential is not applied, many TCF's computed for a duration of time less than the time it would take for a water molecule to diffuse half the length of the simulation box is necessary to obtain an averaged TCF that is easily Fourier transformed. In past studies [6, 38] that did not use a restraining potential, this was the general methodology

for calculating SVFS spectra. However, while the average of the many short time TCF's obtained were Fourier transformable, the signal was noisy to the extent that the location of subpopulations could not be identified.

The reason why using a lateral restraining potential centered in the middle of the box creates a signal with the wrong phase in only an isolated region of the spectrum is because its presence creates an artificial interface that mimics an environment that is similar in nature to the bottom of the first condensed phase water layer at the water/vapor interface. The interface created by the restraining potential is the opposite environment (directionally) of the water/vapor interface, and thus there is competitive (deconstructive) interference in the calculated signal from these two environments. Further, it has been shown [76] that the bottom of the first condensed phase water layer primarily contributes to the 3400 cm^{-1} region, while the top layer accounts for the free OH species. The physical constraints of having a restraining potential do not allow for a free OH species to be created. This why the phase of the free OH was not affected. The new, phase correct, spectra where obtained by neglecting the molecules in the middle third region of the simulation box when calculating the SVFS TCF. This exclusion creates a boundary in the box, but not an interface. Effectively, this boundary acts as a poor man's implicit solvation.

3.3 Concluding Remarks on New Water Model & Future Improvements

In analyzing the polarizability derivative tensor, the average percent error between the ES and BSM is 6.882. The fitted BSM for water reproduces the general polarizability derivative trends, but the percent error of several of these elements is above 10%. This leads to some concern. However, given that the IR, Raman, and phase correct SVFS spectra were reproduced from these parameters, further refinement was not pursued. In the future, it may be desired to refit the polarizability values for the BSM of water as a function of displacement from equilibrium bond length and displacement from the equilibrium bond angle (θ): $\alpha(r,\theta) = \alpha_o + \alpha'_r \Delta r + \alpha'_\theta \Delta\theta$. Another possibility would be to not approximate the polarizability and/or polarizability derivatives to be points, but rather tensors as they are formally given. This later method could then also be parametrized as a function of displacement from equilibrium bond length and/or bond angle.

Chapter 4

Quadrupole Induced Bulk SVFS

As described in Chapter 3, under the usual dipole approximation, second order (three-wave mixing) spectroscopies vanish in isotropic media due to the inversion symmetry of such systems. [2,3,6] Interfaces serve to break this symmetry, and produce a second order polarization signal. Beyond the dipole approximation, the bulk of a system can contribute coherently to second order optical measurements through quadrupole (and higher order) effects. While quadrupole contributions can be several orders of magnitude smaller than dipole effects, [30] the relative number of absorbers in the bulk *vs.* interfacial regions is large – making the collective quadrupole contribution significant in some systems. Note, the quadrupole contributions from the bulk originate in a region that is roughly the wavelength of light used while the interfacial contribution is limited to a few molecular layers. The dynamics between these two regions can be significantly different. [6, 19]

There have been a multitude of careful and interesting interfacial studies of liquid systems – both experimentally [12,53,55,58,60,69,72,77–81] and theoretically [6,19,38,50, 68,82–84] – using SVFS. These studies have typically assumed the dipole approximation

to be adequate in either interpreting or calculating the SVFS signal. Quadrupole contributions have usually, *a priori*, been assumed to be negligible because they are minimized by taking experimental optical measurements in the reflected (as opposed to transmission) geometry (Figure 4). [13] Shen *et. al* have shown there are no established general physical criteria that determine when quadrupole contributions can be neglected, and that they need to be investigated on a case by case basis. [53, 85, 86] Further, while experimental determinations (assessing the differences in the signal in the transmission and reflection geometry) can determine the relative importance of the bulk signal, it is not possible to completely separate the bulk and surface contributions. [86] Also, the importance of bulk contributions is highly dependent on the particular polarization condition that is probed. [85, 86] Thus, in the goal of accurately interpreting three-wave mixing spectra, it is to the benefit of both the experimental and theoretical communities to have a general molecularly detailed technique by which quadrupole contributions to SVFS spectra can be quantified.

Therefore, a molecularly detailed TCF approach for calculating bulk quadrupole contributions to the SVFS spectra that is generally valid has been developed, and is presented in detail below. This chapter concludes with a practical, computationally tractable, implementation model of the theory including permanent and induced quadrupole effects.

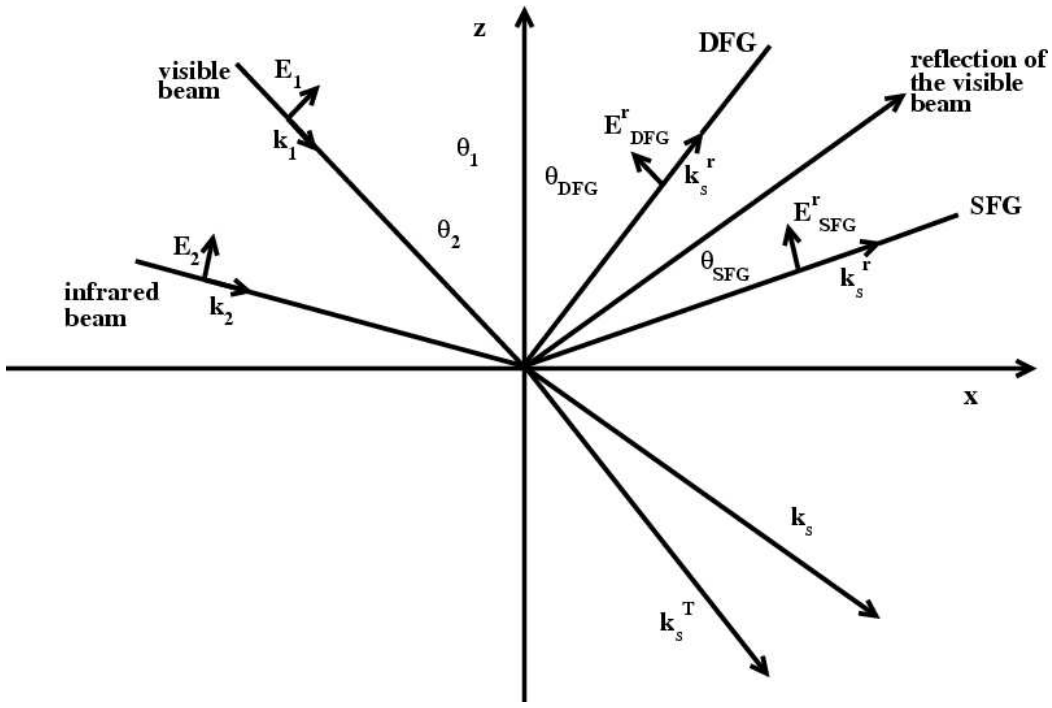

Figure 4.1: Coplanar geometry of the incident, reflected and transmitted beams. θ_1 (θ_2) is the angle of incidence with respect to the z-axis of the visible (IR) field. θ_{SFG} (θ_{DFG}) is the angle the generated SFG (DFG) signal is radiated at. $\mathbf{k}_1$ ($\mathbf{k}_2$) is the wave vector of the visible (IR) field. $\mathbf{k}_s{}^r$ ($\mathbf{k}_s{}^T$) is the wave vector of the reflected (transmitted) field, and $\mathbf{k}_s$ = $\mathbf{k}_1$ + $\mathbf{k}_2$. All incident fields are assumed to lie in the same xz plane which is normal to the surface.

4.1 General Theoretical Development of Quadrupole Contributions

The N^{th} order polarization signal a given spectroscopy measures is proportional to the N^{th} order susceptibility of a system. [2, 3, 6] Therefore, developing a TCF theory of quadrupole contributions to the SVFS spectra requires starting with the general second order susceptibility expression. This process deviates from the theoretical development detailed in Chapter 3 in that it must incorporates both dipole and quadrupole ($\mathbf{q}$) contributions in the perturbed Hamiltonian, $H^{(1)}$. This implies that the total second order polarization is given by:

$$\boldsymbol{P}^{(2)}(\mathbf{r},t) = M\langle\boldsymbol{\mu}\rho^{(2)}\rangle + M \bigtriangledown \langle\boldsymbol{q}\rho^{(2)}\rangle \tag{4.1}$$

To obtain a general expression for the susceptibility that includes both dipole and quadrupole contributions, the orders of the density matrix must be resolved. Rederiving $\rho^{(1)}$, $\rho^{(2)}$, and the now multiple $\boldsymbol{\chi}^{(1)}$ components using $H^{(1)} = -\boldsymbol{\mu}\cdot\boldsymbol{E}(t) - \boldsymbol{q}\cdot\bigtriangledown\boldsymbol{E}(t)$, the total second order polarization in terms of tensor components, including both dipole and quadrupole contributions, can be expressed as:

$$P_i^{(2)} = P_i^{(2),D} + \bigtriangledown_j P_{ij}^{(2),Q} \tag{4.2}$$

$$\begin{aligned} P_i^{(2),D} = {} & \chi_{ijk}^{(2)D} E_j(\omega_q)E_k(\omega_p) + \chi_{ijkl}^{(2)D_{q1}} \frac{\partial E_j(\omega_q)}{\partial r_k} E_l(\omega_p) \\ & + \chi_{ijkl}^{(2)D_{q2}} E_j(\omega_q) \frac{\partial E_k(\omega_p)}{\partial r_l} + \chi_{ijklm}^{(2)D_{q3}} \frac{\partial E_j(\omega_q)}{\partial r_k} \frac{\partial E_l(\omega_p)}{\partial r_m} \end{aligned} \tag{4.3}$$

$$\begin{aligned} P_{ij}^{(2),Q} = {} & \chi_{ijkl}^{(2)Q} E_k(\omega_q)E_l(\omega_p) + \chi_{ijklm}^{(2)Q_{q1}} E_m(\omega_p) \frac{\partial E_k(\omega_q)}{\partial r_l} \\ & + \chi_{ijklm}^{(2)Q_{q2}} E_k(\omega_q) \frac{\partial E_l(\omega_p)}{\partial r_m} + \chi_{ijklmn}^{(2)Q_{q3}} \frac{\partial E_k(\omega_q)}{\partial r_l} \frac{\partial E_m(\omega_p)}{\partial r_n} \end{aligned} \tag{4.4}$$

In Equations 4.2 – 4.4 the Einstein summation notation is implied. Here, $P_i^{(2)}$ is the total second order polarization. $P_i^{(2),D}$ and $P_{ij}^{(2),Q}$ are the dipole and quadrupole moment contributions to the total second order polarization respectively. $P_i^{(2),D}$ contains terms that collectively contribute to $P_i^{(2)}$ linearly, and $P_{ij}^{(2),Q}$ contains terms that collectively contribute to $P_i^{(2)}$ through $P_{ij}^{(2),Q}$'s gradient.

Comparison of the second order dipolar polarization expression derived in Chapter 3 with the components of Equation 4.2 reveals that only the first term in Equation 4.3 is obtained when quadrupole contributions are neglected. Hence, all other terms in Equation 4.2 are inherently quadrupole in origin. Note, the final term in Equation 4.3 and the final three terms in Equation 4.4 have generally been neglected in the literature when quadrupole contributions have been discussed because they are higher order contributions in the sense that they involve multiple gradients, [87, 88] but can be important, especially when considering systems containing physically large components – such as, metallic systems, suspended nanoparticles, or colloids. [14, 15]

The following general expressions for the susceptibilities in Equations 4.3 and 4.4 are given in a form that suppresses the required intrinsic permutation symmetry for brevity; to derive the TCF expressions that follow, the full susceptibility tensors, including intrinsic permutation symmetry, must be considered. Keeping with the notation established in previous chapters, μ_{ab}^i (q_{ab}^i) is a dipole (quadrupole) matrix element between states a and b with a polarization component of i, $\omega_{ab} \equiv \omega_a - \omega_b$, and $\gamma_{ab} = \gamma_{ba}$. γ is a damping factor that controls the linewidth, and is naturally incorporated into the system dynamics.

$$\boldsymbol{\chi}^{(2)D}_{ijk} = \frac{M}{\hbar^2}\sum_{grv}\rho^{(0)}_{vv}\left(\frac{\mu^i_{gv}\mu^k_{vr}\mu^j_{rg}}{(\omega_s+\omega_{gv}+i\gamma_{gv})(\omega_p+\omega_{rv}+i\gamma_{rv})}\right.$$

$$+\frac{\mu^i_{vg}\mu^k_{rv}\mu^j_{gr}}{(\omega_s-\omega_{gv}+i\gamma_{gv})(\omega_p-\omega_{rv}+i\gamma_{rv})}$$

$$-\frac{\mu^i_{rg}\mu^k_{vr}\mu^j_{gv}}{(\omega_s-\omega_{gr}+i\gamma_{gr})(\omega_p+\omega_{rv}+i\gamma_{rv})}$$

$$\left.-\frac{\mu^i_{rg}\mu^k_{gv}\mu^j_{vr}}{(\omega_s-\omega_{gr}+i\gamma_{gr})(\omega_p-\omega_{gv}+i\gamma_{gv})}\right) \tag{4.5}$$

$$\boldsymbol{\chi}^{(2)D_{q1}}_{ijkl} = \frac{M}{\hbar^2}\sum_{grv}\rho^{(0)}_{vv}\left(\frac{\mu^i_{gv}\mu^l_{vr}q^{jk}_{rg}}{(\omega_s+\omega_{gv}+i\gamma_{gv})(\omega_p+\omega_{rv}+i\gamma_{rv})}\right.$$

$$+\frac{\mu^i_{vg}\mu^l_{rv}q^{jk}_{gr}}{(\omega_s-\omega_{gv}+i\gamma_{gv})(\omega_p-\omega_{rv}+i\gamma_{rv})}$$

$$-\frac{\mu^i_{rg}\mu^l_{vr}q^{jk}_{gv}}{(\omega_s-\omega_{gr}+i\gamma_{gr})(\omega_p+\omega_{rv}+i\gamma_{rv})}$$

$$\left.-\frac{\mu^i_{rg}\mu^l_{gv}q^{jk}_{vr}}{(\omega_s-\omega_{gr}+i\gamma_{gr})(\omega_p-\omega_{gv}+i\gamma_{gv})}\right) \tag{4.6}$$

$$\boldsymbol{\chi}^{(2)D_{q2}}_{ijkl} = \frac{M}{\hbar^2}\sum_{grv}\rho^{(0)}_{vv}\left(\frac{\mu^i_{gv}q^{kl}_{vr}\mu^j_{rg}}{(\omega_s+\omega_{gv}+i\gamma_{gv})(\omega_p+\omega_{rv}+i\gamma_{rv})}\right.$$

$$+\frac{\mu^i_{vg}q^{kl}_{rv}\mu^j_{gr}}{(\omega_s-\omega_{gv}+i\gamma_{gv})(\omega_p-\omega_{rv}+i\gamma_{rv})}$$

$$-\frac{\mu^i_{rg} q^{kl}_{vr} \mu^j_{gv}}{(\omega_s - \omega_{gr} + i\gamma_{gr})(\omega_p + \omega_{rv} + i\gamma_{rv})}$$

$$-\frac{\mu^i_{rg} q^{kl}_{gv} \mu^j_{vr}}{(\omega_s - \omega_{gr} + i\gamma_{gr})(\omega_p - \omega_{gv} + i\gamma_{gv})}\Bigg) \tag{4.7}$$

$$\boldsymbol{\chi}^{(2)D_{q3}}_{ijklm} = \frac{M}{\hbar^2}\sum_{grv}\rho^{(0)}_{vv}\Bigg(\frac{\mu^i_{gv} q^{lm}_{vr} q^{jk}_{rg}}{(\omega_s + \omega_{gv} + i\gamma_{gv})(\omega_p + \omega_{rv} + i\gamma_{rv})}$$

$$+\frac{\mu^i_{vg} q^{lm}_{rv} q^{jk}_{gr}}{(\omega_s - \omega_{gv} + i\gamma_{gv})(\omega_p - \omega_{rv} + i\gamma_{rv})}$$

$$-\frac{\mu^i_{rg} q^{lm}_{vr} q^{jk}_{gv}}{(\omega_s - \omega_{gr} + i\gamma_{gr})(\omega_p + \omega_{rv} + i\gamma_{rv})}$$

$$-\frac{\mu^i_{rg} q^{lm}_{gv} q^{jk}_{vr}}{(\omega_s - \omega_{gr} + i\gamma_{gr})(\omega_p - \omega_{gv} + i\gamma_{gv})}\Bigg) \tag{4.8}$$

$$\boldsymbol{\chi}^{(2)Q}_{ijkl} = \frac{M}{\hbar^2}\sum_{grv}\rho^{(0)}_{vv}\Bigg(\frac{q^{ij}_{gv} \mu^l_{vr} \mu^k_{rg}}{(\omega_s + \omega_{gv} + i\gamma_{gv})(\omega_p + \omega_{rv} + i\gamma_{rv})}$$

$$+\frac{q^{ij}_{vg} \mu^l_{rv} \mu^k_{gr}}{(\omega_s - \omega_{gv} + i\gamma_{gv})(\omega_p - \omega_{rv} + i\gamma_{rv})}$$

$$-\frac{q^{ij}_{rg} \mu^l_{vr} \mu^k_{gv}}{(\omega_s - \omega_{gr} + i\gamma_{gr})(\omega_p + \omega_{rv} + i\gamma_{rv})}$$

$$-\frac{q^{ij}_{rg} \mu^l_{gv} \mu^k_{vr}}{(\omega_s - \omega_{gr} + i\gamma_{gr})(\omega_p - \omega_{gv} + i\gamma_{gv})}\Bigg) \tag{4.9}$$

$$\boldsymbol{\chi}^{(2)Q_{q_1}}_{ijklm} = \frac{M}{\hbar^2}\sum_{grv}\rho^{(0)}_{vv}\Bigg(\frac{q^{ij}_{gv} \mu^m_{vr} q^{kl}_{rg}}{(\omega_s + \omega_{gv} + i\gamma_{gv})(\omega_p + \omega_{rv} + i\gamma_{rv})}$$

$$+\frac{q^{ij}_{vg}\mu^{m}_{rv}q^{kl}_{gr}}{(\omega_s-\omega_{gv}+i\gamma_{gv})(\omega_p-\omega_{rv}+i\gamma_{rv})}$$

$$-\frac{q^{ij}_{rg}\mu^{m}_{vr}q^{kl}_{gv}}{(\omega_s-\omega_{gr}+i\gamma_{gr})(\omega_p+\omega_{rv}+i\gamma_{rv})}$$

$$-\frac{q^{ij}_{rg}\mu^{m}_{gv}q^{kl}_{vr}}{(\omega_s-\omega_{gr}+i\gamma_{gr})(\omega_p-\omega_{gv}+i\gamma_{gv})}\Bigg) \tag{4.10}$$

$$\boldsymbol{\chi}^{(2)Q_{q_2}}_{ijklm}=\frac{M}{\hbar^2}\sum_{grv}\rho^{(0)}_{vv}\left(\frac{q^{ij}_{gv}q^{lm}_{vr}\mu^{k}_{rg}}{(\omega_s+\omega_{gv}+i\gamma_{gv})(\omega_p+\omega_{rv}+i\gamma_{rv})}\right.$$

$$+\frac{q^{ij}_{vg}q^{lm}_{rv}\mu^{k}_{gr}}{(\omega_s-\omega_{gv}+i\gamma_{gv})(\omega_p-\omega_{rv}+i\gamma_{rv})}$$

$$-\frac{q^{ij}_{rg}q^{lm}_{vr}\mu^{k}_{gv}}{(\omega_s-\omega_{gr}+i\gamma_{gr})(\omega_p+\omega_{rv}+i\gamma_{rv})}$$

$$-\frac{q^{ij}_{rg}q^{lm}_{gv}\mu^{k}_{vr}}{(\omega_s-\omega_{gr}+i\gamma_{gr})(\omega_p-\omega_{gv}+i\gamma_{gv})}\Bigg) \tag{4.11}$$

$$\boldsymbol{\chi}^{(2)Q_{q_3}}_{ijklmn}=\frac{M}{\hbar^2}\sum_{grv}\rho^{(0)}_{vv}\left(\frac{q^{ij}_{gv}q^{mn}_{vr}q^{kl}_{rg}}{(\omega_s+\omega_{gv}+i\gamma_{gv})(\omega_p+\omega_{rv}+i\gamma_{rv})}\right.$$

$$+\frac{q^{ij}_{vg}q^{mn}_{rv}q^{kl}_{gr}}{(\omega_s-\omega_{gv}+i\gamma_{gv})(\omega_p-\omega_{rv}+i\gamma_{rv})}$$

$$-\frac{q^{ij}_{rg}q^{mn}_{vr}q^{kl}_{gv}}{(\omega_s-\omega_{gr}+i\gamma_{gr})(\omega_p+\omega_{rv}+i\gamma_{rv})}$$

$$-\frac{q^{ij}_{rg}q^{mn}_{gv}q^{kl}_{vr}}{(\omega_s-\omega_{gr}+i\gamma_{gr})(\omega_p-\omega_{gv}+i\gamma_{gv})}\Bigg) \tag{4.12}$$

4.2 TCF Expressions for SVFS Quadrupolar Susceptibilities

The general second order susceptibilities presented above, including intrinsically permutated terms, represent a starting point for deriving unique quantum mechanical TCF's that describe the response of a particular type of spectroscopy. Henceforth, focus will be exclusively on the resonant portion of the various second order susceptibilities. This is because these portions provide the dominant, and most informative, contribution to the resonant SVFS spectral lineshape. In this derivation, we are guided by the fact that all time domain response functions must be purely real. [5, 89]

To recast the second order susceptibility tensors in terms of correlation functions describing SVFS, the dipole (α), dipole-quadrupole (Φ, $\tilde{\Phi}$), and quadrupole (Υ) polarizabilities, as defined by the first order solution to the density matrix (derivation not shown), will be used. These are defined as:

$$\alpha^{ab}(\omega) = \frac{1}{\hbar}\sum_{vn}\rho_{vv}\left\{\frac{\mu^a_{vn}\mu^b_{nv}}{\omega_{nv}-\omega-i\gamma_{nv}}+\frac{\mu^b_{vn}\mu^a_{nv}}{\omega_{nv}+\omega+i\gamma_{nv}}\right\} \tag{4.13}$$

$$\tilde{\Phi}^{abc}(\omega) = \frac{1}{\hbar}\sum_{vn}\rho_{vv}\left\{\frac{\mu^a_{vn}q^{bc}_{nv}}{\omega_{nv}-\omega-i\gamma_{nv}}+\frac{\mu^a_{nv}q^{bc}_{vn}}{\omega_{nv}+\omega+i\gamma_{nv}}\right\} \tag{4.14}$$

$$\Phi^{abc}(\omega) = \frac{1}{\hbar}\sum_{vn}\rho_{vv}\left\{\frac{q^{ab}_{vn}\mu^c_{nv}}{\omega_{nv}-\omega-i\gamma_{nv}}+\frac{\mu^a_{vn}q^{ab}_{nv}}{\omega_{nv}+\omega+i\gamma_{nv}}\right\} \tag{4.15}$$

$$\Upsilon^{abef}(\omega) = \frac{1}{\hbar}\sum_{vn}\rho_{vv}\left\{\frac{q^{ab}_{vn}q^{ef}_{nv}}{\omega_{nv}-\omega-i\gamma_{nv}}+\frac{q^{ab}_{nv}q^{ef}_{vn}}{\omega_{nv}+\omega+i\gamma_{nv}}\right\} \tag{4.16}$$

First, the resonant components of $\boldsymbol{\chi}^{(2)D}_{ijk}$, $\boldsymbol{\chi}^{(2)Dq3}_{ijklm}$, $\boldsymbol{\chi}^{(2)Q}_{ijkl}$, and $\boldsymbol{\chi}^{(2)Qq3}_{ijklmn}$ are considered. In pursuit of developing computationally amenable TCF expressions, the following assumptions are made: (1) $\gamma_{rv}+\gamma_{gv}\approx\gamma_{gr}$, (2) $1/\omega_s \approx 1/\omega_p$, and (3) (where applicable) field

derivatives terms are symmetric in the sense that $\frac{\partial E_a}{\partial r_b} = \frac{\partial E_b}{\partial r_a}$. Note for SVFS, the first approximation amounts to equating the frequency of the sum and visible fields, and both the first and second approximations are required to derive the well-known [6, 50] SVFS TCF that describes the system response in the dipole approximation.

Letting $\boldsymbol{\chi}^{(2),RES}$ denote only the resonant portion of the susceptibility:

$$\boldsymbol{\chi}^{(2)D,RES}_{ijk} = \frac{1}{\hbar}\sum_{vgr}\rho^{(0)}_{vv}\left\{\frac{\mu^j_{rv}\alpha^{ik}_{vr}(\omega_s)}{(\omega_q-\omega_{gv}+i\gamma_{gv})}+\frac{\alpha^{ik}_{rv}(\omega_s)\mu^j_{vr}}{\omega_q+\omega_{gv}+i\gamma_{gv}}\right\} \tag{4.17}$$

$$= \frac{i}{\hbar}\int_0^\infty dt\, e^{(i\omega_q t)} < \alpha^{ik}(t)\mu^j(0) > -\frac{i}{\hbar}\int_0^\infty dt\, e^{(i\omega_q t)} < \mu^j(0)\alpha^{ik}(t) > \tag{4.18}$$

In deriving Equation 4.18 from Equation 4.17, the integral identity $-i\int_0^\infty dt\, e^{it(a+ib)} = 1/(a+ib)$ is used to replace the denominators in Equation 4.17, the definition of the Heisenberg representation of a time dependent operator is applied to obtain $\alpha(t)$, and the necessary sums over states are performed. TCF expressions for $\boldsymbol{\chi}^{(2)D_{q3}}_{ijklm}$, $\boldsymbol{\chi}^{(2)Q}_{ijkl}$, and $\boldsymbol{\chi}^{(2)Q_{q_3}}_{ijklmn}$ are derived in an analogous fashion, *i.e.* making the same approximations necessary to develop Equation 4.18.

$$\boldsymbol{\chi}^{(2)D_{q3},RES}_{ijklm} = \frac{i}{\hbar}\int_0^\infty dt\, e^{(i\omega_q t)}\left[< \tilde{\Phi}^{ilm}(t)q^{jk}(0) > - < q^{jk}(0)\tilde{\Phi}^{ilm}(t) >\right] \tag{4.19}$$

$$\boldsymbol{\chi}^{(2)Q,RES}_{ijkl} = \frac{i}{\hbar}\int_0^\infty dt\, e^{(i\omega_q t)}\left[< \Phi^{ijk}(t)\mu^l(0) > - < \mu^l(0)\Phi^{ijk}(t) >\right] \tag{4.20}$$

$$\boldsymbol{\chi}^{(2)Q_{q_3},RES}_{ijklmn} = \frac{i}{\hbar}\int_0^\infty dt\, e^{(i\omega_q t)}\left[< \Upsilon^{ijmn}(t)q^{kl}(0) > - < \mu^{kl}(0)\Upsilon^{ijmn}(t) >\right] \tag{4.21}$$

Additional simplification of Equations 4.18-4.21 is possible by writing the complex correlation functions, generally denoted by $C(t)$, describing the resonant susceptibilities

in terms of their real, $C_R(t)$, and imaginary, $C_I(t)$, parts; $C(t) = C_R(t) + iC_I(t)$. When expanded out in such a manner, the resonant frequency dependent susceptibilities can be written as a half-sided transform over their time dependent imaginary component. [6, 52] This satisfies the necessary requirement that a time dependent response function is purely real. [89, 90]

As was discussed in Chapter 3, the imaginary component of a correlation function cannot be directly calculated *via* classical computation techniques – it is only the classical limit of the real part of the complex correlation function that can be calculated directly. However, as shown in Chapter 3, all two-point, one-time, TCF's have an analytical detailed balance relationship between their real and imaginary parts in the frequency domain given by: $C_R(\omega) = cotanh(\beta\hbar\omega/2)C_I(\omega)$. Substitution of this relationship into the various resonant susceptibility expressions establishes a definitive quantum-classical correspondence, and provides a direct route for calculating the microscopic susceptibilities and spectra for systems of interest.

$\boldsymbol{\chi}^{(2)D_{q1}}_{ijkl}$, $\boldsymbol{\chi}^{(2)D_{q2}}_{ijkl}$, $\boldsymbol{\chi}^{(2)Q_{q_1}}_{ijklm}$, and $\boldsymbol{\chi}^{(2)Q_{q_2}}_{ijklm}$ can also each be written in terms of a half sided transform of the difference of two TCF's that are complex conjugates. The rewrite of these four terms requires a slightly different, but relatively similar, set of approximations; $\omega_s \pm \omega_{gr} \approx \omega_s \pm \omega_{gv}$ which is reasonable under typical thermal experimental conditions, and field derivatives terms are assumed to be symmetric in the sense that $\frac{\partial E_a}{\partial r_b} = \frac{\partial E_b}{\partial r_a}$. Note, in addition to the above method, the resonant portion of $\boldsymbol{\chi}^{(2)D}_{ijk}$, $\boldsymbol{\chi}^{(2)D_{q3}}_{ijklm}$, $\boldsymbol{\chi}^{(2)Q}_{ijkl}$, and $\boldsymbol{\chi}^{(2)Q_{q_3}}_{ijklmn}$ can also be written in terms of TCF's using this set of approximations. In this case, the

resulting expressions for their resonant susceptibilities are still described by Equations 4.18 – 4.21. The resonant susceptibility for $\boldsymbol{\chi}_{ijkl}^{(2)D_{q1}}$, $\boldsymbol{\chi}_{ijkl}^{(2)D_{q2}}$, $\boldsymbol{\chi}_{ijklm}^{(2)Q_{q_1}}$, and $\boldsymbol{\chi}_{ijklm}^{(2)Q_{q_2}}$ are given by:

$$\boldsymbol{\chi}_{ijkl}^{(2)D_{q1},RES} = \frac{i}{\hbar}\int_0^\infty dt\; e^{iw_q t}\left\{< \tilde{\Phi}^{ikl}(t)\mu^j(0) > - < \mu^j(0)\tilde{\Phi}^{ikl}(t) >\right\} \tag{4.22}$$

$$\boldsymbol{\chi}_{ijkl}^{(2)D_{q2},RES} = \frac{i}{\hbar}\int_0^\infty dt\; e^{iw_q t}\left\{< \alpha^{il}(t)q^{jk}(0) > - < q^{jk}(0)\alpha^{il}(t) >\right\} \tag{4.23}$$

$$\boldsymbol{\chi}_{ijklm}^{(2)Q_{q_1},RES} = \frac{i}{\hbar}\int_0^\infty dt\; e^{iw_q t}\left\{< \Upsilon^{ijlm}(t)\mu^k(0) > - < \mu^k(0)\Upsilon^{ijlm}(t) >\right\} \tag{4.24}$$

$$\boldsymbol{\chi}_{ijklm}^{(2)Q_{q_2},RES} = \frac{i}{\hbar}\int_0^\infty dt\; e^{iw_q t}\left\{< \Phi^{ijm}(t)q^{kl}(0) > - < q^{kl}(0)\Phi^{ijm}(t) >\right\} \tag{4.25}$$

Equations 4.19 – 4.25 are TCF formulas that are capable of describing the quadrupole contributions to the resonant spectral lineshape at all frequencies – avoiding the rotating wave approximation which has been previously used [87] to describe only high frequency quadrupole SVFS contributions. Next, a novel microscopic polarizability model is presented to permit the calculation of the above TCF's that is compatible with MD simulations.

4.3 Calculation *via* a Charge-Interaction Model

The BSM, which includes calculation of the total system dipole and polarizability, has been previously outlined in Chapter 2. The fitting of and application to an interfacial liquid system of the BSM was also presented in Chapter 3. The BSM must be further

extended to calculate the total system quadrupole, dipole-quadrupole, and quadrupole polarizabilities. In addition to the total dipole and polarizability, these quantities are also necessary for calculation of quadrupole-origin SVFS TCF's. All three new quantities can be determined by a novel generalization of the BSM outlined in Chapters 2 and 3. The remainder of this section will systematically detail the equations that need to be computationally implemented within a spectroscopic model to obtain the requisite additional electric moment and electric moment polarizabilities.

Note, the results presented in this section are all in terms of Cartesian tensor components (superscript Greek indices) for a single atom (Roman indices). The various molecular polarizabilities are a sum of all their atomic polarizabilities, repeated Greek indices are to be summed over, subscripts of o denote permanent/intrinsic moments, and $T_{ij}^{\alpha\beta\ldots\zeta}$ is the multipole interaction tensor given by: $\bigtriangledown_\alpha \bigtriangledown_\beta .. \bigtriangledown_\zeta \ (1/\mathbf{r}_{ij})$ where $\mathbf{r}_{ij}$ is the vector between atom i and atom j. [46, 91] E_i^α ($E_i^{\alpha\beta}$) is a field (field gradient) including both local and external field contributions whereas $E_{i,o}^\alpha$ ($E_{i,o}^{\alpha\beta}$) denotes an external field (field gradient).

Within an extended BSM (also referred to as a PAPA model), the induced dipole is given by Equation 4.26. Beyond the dipole approximation, the individual induced dipole moments also have a quadrupole contribution. This contribution is represented by the third term of Equation 4.26. [92] In the common dipole approximation expression, only the first two terms on the right hand side are obtained.

$$\mu_i^\alpha = \alpha E_i^\alpha = \alpha_{i,o} E_o^\alpha + \alpha_{i,o} \sum_j T_{ij}^{\alpha\beta} \mu_j^\beta - \frac{\alpha_{i,o}}{3} \sum_j T_{ij}^{\alpha\beta\gamma} q_j^{\beta\gamma} \tag{4.26}$$

From Equation 4.26, a super-matrix detailing the effective polarizability, $\alpha_{ij}^{\alpha\beta}$, between every atom pair in the system can be solved for. [46]

The induced quadrupole is given by:

$$q_i^{\alpha\beta} = \Phi_i^{\alpha\beta\gamma} E_i^{\gamma} + \Upsilon_i^{\alpha\beta\gamma\zeta} E_i^{\gamma\zeta} \tag{4.27}$$

Notice, the induced quadrupole includes contributions from both the dipole-quadrupole, Φ, and pure quadrupole, Υ, polarizabilities. The induced dipole-quadrupole and pure quadrupole moments have been demonstrated to be important in, *e.g.*, ice. [93]

The induced dipole-quadrupole contribution to the quadrupole and dipole-quadrupole polarizability can be calculated in terms of Equations 4.28 and 4.29. [46,94] Alternatively, the numerical derivative of the total quadrupole with respect to the field can be taken to obtain the dipole-quadrupole polarizability. The necessary modification of Equation 4.29 to obtain $\tilde{\Phi}^{\alpha\beta\gamma}$ (see Equations 4.15 and 4.14) is straightforward.

$$\Phi_i^{\alpha\beta\gamma} E_i^{\gamma} = \Phi_i^{\alpha\beta\gamma} E_{i,o}^{\gamma} \Phi_i^{\alpha\beta\gamma} \sum_j T_{ij}^{\gamma\zeta} \mu_j^{\zeta} - \frac{\Phi_i^{\alpha\beta\gamma}}{3} \sum_j T_{ij}^{\gamma\zeta\eta} q_j^{\zeta\eta} \tag{4.28}$$

$$\Phi_{ij}^{\alpha\beta\gamma} = \frac{3}{2} r_i^{\beta} \alpha_i^{\alpha\gamma} + \frac{3}{2} r_i^{\alpha} \alpha_i^{\beta\gamma} - \frac{1}{2} r_i^{\alpha} \alpha_i^{\alpha\gamma} \delta_{\alpha\beta} \tag{4.29}$$

The induced quadrupole due to the quadrupole polarizability and quadrupole polarizability are given by Equations 4.30 and 4.31 respectively. [94, 95] Alternatively, the numerical derivative of the total quadrupole with respect to the field gradient can be taken to obtain the pure quadrupole polarizability.

$$\Upsilon_i^{\alpha\beta\gamma\zeta} E_i^{\gamma\zeta} = \Upsilon_i^{\alpha\beta\gamma\zeta} E_{i,o}^{\gamma\zeta} + \Upsilon_i^{\alpha\beta\gamma\zeta} \sum_j T_{ij}^{\gamma\zeta\delta} \mu_j^{\delta} - \frac{\Upsilon_i^{\alpha\beta\gamma\zeta}}{3} \sum_j T_{ij}^{\gamma\zeta\delta\pi} q_j^{\delta\pi} \tag{4.30}$$

$$2\Upsilon_i^{\alpha\beta\gamma\zeta} = r_i^{\alpha}\Phi_i^{\beta\gamma\zeta} + r_i^{\beta}\Phi_i^{\alpha\gamma\zeta} - \frac{2}{3}r_i^{\epsilon}\Phi_i^{\epsilon\gamma\zeta}\delta_{\alpha\beta} + r_i^{\gamma}\Phi_i^{\zeta\alpha\beta} + r_i^{\zeta}\Phi_i^{\gamma\alpha\beta} - \frac{2}{3}r_i^{\epsilon}\Phi_i^{\epsilon\alpha\beta}\delta_{\gamma\zeta}$$

$$-\frac{3}{2}r_i^{\alpha}r_i^{\gamma}\alpha_i^{\beta\zeta} - \frac{3}{2}r_i^{\alpha}r_i^{\zeta}\alpha_i^{\beta\gamma} + r_i^{\alpha}r_i^{\epsilon}\delta_{\gamma\zeta}\alpha_i^{\epsilon\beta} - \frac{3}{2}r_i^{\beta}r_i^{\gamma}\alpha_i^{\zeta\alpha} - \frac{3}{2}r_i^{\beta}r_i^{\zeta}\alpha_i^{\alpha\gamma}$$

$$+r_i^{\beta}r_i^{\epsilon}\delta_{\gamma\zeta}\alpha_i^{\epsilon\alpha} + r_i^{\epsilon}r_i^{\gamma}\delta_{\alpha\beta}\alpha_i^{\epsilon\zeta} + r_i^{\epsilon}r_i^{\zeta}\delta_{\alpha\beta}\alpha_i^{\epsilon\gamma} - \frac{2}{3}r_i^{\epsilon}r_i^{\pi}\delta_{\alpha\beta}\delta_{\gamma\beta}\alpha_i^{\epsilon\pi} \tag{4.31}$$

In Equation 4.30, the multipole interaction tensors $T_{ij}^{\gamma\zeta\delta}$ and $T_{ij}^{\gamma\zeta\delta\pi}$ are third and fourth tensors respectively for every atom interaction pair ij. These can be computationally expensive to calculate. However, the computational expense can be significantly reduced by: (1) exploiting the non-uniqueness of many of the elements present in the multipole interaction tensor for a given rank, and (2) using a recursive relationship to generate the N rank interaction tensor from the $N-1$ rank tensor. [96] Additionally, symmetries are present in the dipole-quadrupole polarizability: $\Phi^{\alpha\beta\gamma}$, (pure-quadrupole polarizability $\Upsilon^{\alpha\beta\gamma\zeta}$) is symmetric in α and β (α and β, γ and ζ). [94] Despite many simplifications, the computational implementation of this extended BSM is a sizable project. Thus, it will be the subject of future work and continued ongoing refinements to the Space Research group spectroscopic model.

Chapter 5

Static Field Induced Third Order SVFS

Liquid interfaces are abundant in chemistry and the environment, and it is common to have charged species or charged solids surfaces present at these interfaces. Charged species can be, *e.g.*, surfactants or any other amphiphile, and a ubiquitous example of a charged solid/liquid interface is the silica/water interface. [97–99] Silicates are common in both the soil and atmospheric dust where many important chemical processes occur. [100, 101] Interfaces of this nature (silica/water) play a critical role in binding pollutants and biological molecules, such as hexavalent chromium, the agricultural antibiotic Morantel, and organic phosphate compounds. [79, 99, 102–104] The charge associated with the silica/water interface is primarily due to the silanol groups, SiOH, which terminate silica. These groups ionize in water – especially as pH is increased, [102, 105, 106] and even the undissociated silica surface produces a relatively large static field due to large charge separation between the atoms (silicon, oxygen, and hydrogen). [102, 104]

Given the prevalent nature of charged interfaces, and the increasing use of second order optical techniques to interrogate interfaces, a question naturally arises: how does the

static field associated with a charged surface modify what an SVFS experiment is fundamentally probing? While a mathematical description of SVFS at a charged interface will be addressed in the following sections, the answer to this question is easy to conceptualize. Specifically, the presence of a static field associated with a charged interface will both produce a more intense second order signal (due to ordering at the interface), and a distinct third order signal (due to contributions from regions into which the static field penetrates). The caveat of SVFS at charged interfaces is that these two distinct contributions are unable to be independently resolved experimentally, but indeed have different physical origins. [6, 19, 34, 96] Further, there is suggestive evidence in the literature of the importance/relative magnitude of this third order contribution, but no previous molecularly detailed approach existed to separately calculate the second and third order contributions. The first molecularly detailed TCF approach that allows for the second and third order contributions to SVFS to be individually determined is presented in the following section. Practical implementation procedures of the derived TCF's that describe these separate phenomenon is subsequently discussed. The Chapter concludes with results of the discussed model applied to a water molecule and a water dimer system.

5.1 Effective Polarization Due to A Static Field in Isotropic Media

In the limit of monochromatic fields, the effective observed polarization, $\mathbf{P}^{eff}$, for a general second order optical experiment at a charged interface (typical referred to as Electric

Field Enhanced SHG/SFG/DFG) is given by: [105–110]

$$\mathbf{P}^{eff} = \mathbf{P}^{(2)} + \mathbf{P}^{(3)} = \boldsymbol{\chi}^{(2)} \mid \mathbf{E}_1\mathbf{E}_2 + \boldsymbol{\chi}^{(3)} \mid \mathbf{E}_1\mathbf{E}_2\mathbf{E}_{static} \tag{5.1}$$

Here, $\mathbf{E}_{static}$, represents the static field, and is completely general at this point; meaning it can be externally applied or an intrinsic characteristic of chemical medium. [105–107, 111] (It should be noted that spectroscopic techniques employing external static electric fields have been used in interfacial studies of solids since the 1960's, [23, 112] but it has not been until more recently that analysis of liquids at intrinsically charged interfaces have become more common. [105, 108, 110, 111, 113–115]) In Equation 5.1, both the second order and third order polarizations contribute coherently to $\mathbf{P}^{eff}$, and directly probe the second and third order susceptibilities respectively. Thus, Equation 5.1 implies the measured polarization signal, in addition to the normal second order signal, contains two other significant contributions. (1) The presence of three fields (two incident + static) gives rise to a third order nonlinear polarization which is not strictly interface specific. (2) The symmetry is broken by the presence of $\mathbf{E}_{static}$, and, thus, it further extends the anisotropic interfacial region into normally centrosymmetric regions of the bulk. [107, 110] (1) directly probes the third order susceptibility. (2) results in an intensification of the second order susceptibility. [105, 106] Hence, these additional contributions to the observed polarization are sensitive to the extended interfacial region resulting from the static field. [107] The advantage of electric field enhanced three-wave mixing investigations lies is their ability to deduce the electrostatic potential created by the charged species near the interface, and monitor how their electrostatic potential changes the na-

ture of the interface; [105, 106] this capability critically relies on separating the second and third order polarization contributions.

Note, $\mathbf{P}^{eff}$ constitutes a combined measurement of second and third order processes due to the wave vector of the static field being zero. A field's wave vector is proportional to its frequency, and the experimentally detected polarization signal is determined by the sum of the perturbing fields' wave vectors. [2, 4, 6] Thus, the two perturbing applied SHG/SFG/DFG fields have non-zero wave vectors, $\mathbf{k_1}$ and $\mathbf{k_2}$, while the static field has a wave vector of zero. This implies the $\mathbf{P}^{(2)}$ and $\mathbf{P}^{(3)}$ signals are generated in the direction: $\mathbf{k}_{signal} = \mathbf{k_1} + \mathbf{k_2}$ and $\mathbf{k}_{signal} = \mathbf{k_1} + \mathbf{k_2} + 0$ respectively.

5.2 Microscopic $\chi^{(3)}$ Expression to Account for a Static Field

Frequency domain perturbative expressions describing the N^{th} order susceptibility can be found in the literature, [2–4] and can be used as the starting point in developing a TCF theory. [6, 50, 87] However, when any of the fields are of zero frequency, the expressions describing the N^{th} order susceptibility appear to contain terms that, under specific conditions, can become secular divergences. (These apparent divergences can also occur when any set of the applied fields frequency's sum to zero.) The case of secular divergence is distinct from analyzing perturbative expressions for divergent terms to assess the dominant/resonant contributions to the N^{th} order susceptibility. Specifically, when field frequencies sum to zero, no resonance condition is met, and it is termed a secular divergence.

Consider for example the typical form of denominators in frequency dependent susceptibility expressions: $1/(\omega_{rg} - \omega_i - i\gamma_{rg})$. While both the secular and resonant terms are divergent, a resonance occurs when the experimental field(s), ω_i, is of the same frequency as a transition, ω_{rg}, – both of which are individually nonzero. A secular divergence appears in this example when ω_i is of zero frequency, and the transition between states is also of zero frequency – i.e., $\omega_{rg} = \omega_{rg}\delta_{rg} = 0$. As shown by Yuratich [116] and Ward [117] *et. al* using the Method of Averages, the apparent secular nature of $\boldsymbol{\chi}^{(N)}$ when any subset of the applied fields sum to zero vanishes. In our analysis of the perturbative expression for SVFS $\boldsymbol{\chi}^{(3)}$, including all forty-eight terms (expression not shown), in the presence of a static field, we have also found all secularly divergent terms that would appear to contribute to the resonant susceptibility exactly cancel out one another. While this result was expected, it provides a useful and necessary check of our methods. Following, the remaining 16, non-secular, resonant contributors to the third order SVFS susceptibility will be given.

Even with the elimination of two thirds the terms, the following derivation is tedious, and the present approach is different than the more common Louiville space approach. [5] To make a connection between the present method [6,6,50,87] and alternative approaches, an equivalent derivation of the well known correspondence between third order optical Kerr effect (OKE) spectroscopy and the linear Raman experiment is given in Chapter 6. This chapter shows how the third order OKE signal is, like the linear Raman measurement, determined by the autocorrelation of the system's polarizability. Chapter 6 also serves to

clarify the different approximations involved when resonant and off-resonant fields are present.

Equation 5.2 defines the third order polarization, $P_k^{(3)}$, in the limit of monochromatic fields and in terms of its' Cartesian tensor components.

$$P_k^{(3)} = \chi_{kjih}^{(3)} E_j(\omega_1) E_i(\omega_2) E_h(\omega_3) \tag{5.2}$$

For the purposes of describing third order SVFS, ω_1, ω_2, and ω_3 are chosen to represent the visible field, infrared field, and static field respectively. Further, $\omega_s = \omega_1 + \omega_2 + \omega_3$ and is the signal frequency while $\omega_{SVFS} = \omega_1 + \omega_2$ and is the sum frequency field. In SVFS spectroscopy, it is only the infrared field that is resonant; both the signal and visible field fall far from resonance.

Because the third field is static $\omega_3 \longrightarrow 0$ and $\omega_{SVFS} = \omega_s$. Given the coupling of the infrared and visible fields to a static field, the *resonant* portion of the third order susceptibility tensor is given by :

$$\chi_{kjih}^{(3),RES} = \sum_{gmnv} \frac{-\rho_{gg}}{\hbar^3}$$

$$\left\{ (1a) \frac{\mu_{gv}^i \mu_{vn}^j \mu_{nm}^k \mu_{mg}^h}{(\omega_{nm} + \omega_s + i\gamma_{nm})(\omega_{mv} - \omega_2 - i\gamma_{mv})(\omega_{vg} + \omega_2 + i\gamma_{vg})} \right.$$
$$+(1b) \frac{\mu_{gv}^i \mu_{vn}^h \mu_{nm}^j \mu_{mg}^k}{(\omega_{vg} + \omega_2 + i\gamma_{vg})(\omega_{ng} + \omega_2 + i\gamma_{ng})(\omega_{mg} + \omega_s + i\gamma_{mg})}$$
$$+(2a) \frac{\mu_{gv}^k \mu_{vn}^j \mu_{nm}^h \mu_{mg}^i}{(\omega_{vg} - \omega_s - i\gamma_{vg})(\omega_{ng} - \omega_2 - i\gamma_{ng})(\omega_{mg} - \omega_2 - i\gamma_{mg})}$$
$$+(2b) \frac{\mu_{gv}^h \mu_{vn}^j \mu_{nm}^k \mu_{mg}^i}{(\omega_{nm} + \omega_s + i\gamma_{vg})(\omega_{vm} + \omega_2 + i\gamma_{ng})(\omega_{mg} - \omega_2 - i\gamma_{mg})}$$
$$+(3a) \frac{\mu_{gv}^i \mu_{vn}^k \mu_{nm}^j \mu_{mg}^h}{(\omega_{nv} - \omega_s - i\gamma_{nv})(\omega_{mv} - \omega_2 - i\gamma_{mv})(\omega_{vg} + \omega_2 + i\gamma_{vg})}$$

$$
\begin{aligned}
&+(3b)\frac{\mu^h_{gv}\mu^k_{vn}\mu^j_{nm}\mu^i_{mg}}{(\omega_{nv}-\omega_s-i\gamma_{nv})(\omega_{vm}+\omega_2+i\gamma_{vm})(\omega_{mg}-\omega_2-i\gamma_{mg})}\\
&+(4a)\frac{\mu^i_{gv}\mu^h_{vn}\mu^k_{nm}\mu^j_{mg}}{(\omega_{mn}-\omega_s-i\gamma_{mn})(\omega_{ng}+\omega_2+i\gamma_{ng})(\omega_{vg}+\omega_2+i\gamma_{vg})}\\
&+(4b)\frac{\mu^j_{gv}\mu^k_{vn}\mu^h_{nm}\mu^i_{mg}}{(\omega_{vn}+\omega_s+i\gamma_{vn})(\omega_{ng}-\omega_2-i\gamma_{ng})(\omega_{mg}-\omega_2-i\gamma_{mg})}\\
&+(5a)\frac{\mu^i_{gv}\mu^h_{vn}\mu^k_{nm}\mu^j_{mg}}{(\omega_{nm}+\omega_s+i\gamma_{nm})(\omega_{mv}-\omega_s-i\gamma_{mv})(\omega_{vg}+\omega_2+i\gamma_{vg})}\\
&+(5b)\frac{\mu^i_{gv}\mu^j_{vn}\mu^h_{nm}\mu^k_{mg}}{(\omega_{ng}+\omega_s+i\gamma_{ng})(\omega_{mg}+\omega_s+i\gamma_{mg})(\omega_{vg}+\omega_2+i\gamma_{mg})}\\
&+(6a)\frac{\mu^i_{gv}\mu^k_{vn}\mu^h_{nm}\mu^j_{mg}}{(\omega_{nv}-\omega_s+i\gamma_{nv})(\omega_{mv}-\omega_s-i\gamma_{mv})(\omega_{vg}+\omega_2+i\gamma_{vg})}\\
&+(6b)\frac{\mu^i_{gv}\mu^j_{vn}\mu^k_{nm}\mu^h_{mg}}{(\omega_{ng}+\omega_s+i\gamma_{ng})(\omega_{mn}-\omega_s-i\gamma_{mn})(\omega_{vg}+\omega_2+i\gamma_{vg})}\\
&+(7a)\frac{\mu^k_{gv}\mu^h_{vn}\mu^j_{nm}\mu^i_{mg}}{(\omega_{ng}-\omega_s-i\gamma_{ng})(\omega_{vg}-\omega_s-i\gamma_{vg})(\omega_{mg}-\omega_2-i\gamma_{mg})}\\
&+(7b)\frac{\mu^j_{gv}\mu^h_{vn}\mu^k_{nm}\mu^i_{mg}}{(\omega_{nm}+\omega_s+i\gamma_{nm})(\omega_{vm}+\omega_s+i\gamma_{vm})(\omega_{mg}-\omega_2-i\gamma_{mg})}\\
&+(8a)\frac{\mu^j_{gv}\mu^k_{vn}\mu^h_{nm}\mu^i_{mg}}{(\omega_{nv}-\omega_s-i\gamma_{vg})(\omega_{vm}+\omega_s+i\gamma_{vm})(\omega_{mg}-\omega_2-i\gamma_{mg})}\\
&+(8b)\frac{\mu^h_{gv}\mu^k_{vn}\mu^j_{nm}\mu^i_{mg}}{(\omega_{vn}+\omega_s+i\gamma_{vn})(\omega_{ng}-\omega_s-i\gamma_{ng})(\omega_{mg}-\omega_2-i\gamma_{mg})}\Bigg\}
\end{aligned}
\tag{5.3}
$$

Here, the alphanumeric labels in parenthesis enumerate subsets of terms within Equation 5.3. Notice there are doubly and singly resonant terms in Equation 5.3. The doubly resonant terms are identified as those that contain two factors of ω_2 in the denominator. The doubly resonant terms describe a resonant enhancement coupling to the static field and then to the visible field. The singly resonant terms describe the sum frequency generated field coupling to the static field. (This ordering of the fields can more easily be seen by representing the frequency domain perturbative expressions as their Fourier-Laplace transform of their corresponding time-dependent expression.) Given, the frequency do-

main expression in Equation 5.3, one can now proceed to simplify the expression by grouping sets of terms to form polarizabilities, and subsequently transforming the resulting TCF expressions into the time domain.

5.3 A TCF Approach to Quantify $\chi^{(3),RES}$ Contributions

Beginning from the microscopic expression in Equation 5.3, a TCF approach for calculating third order contributions to the SVFS signal is derived that describes the third order effects due to the presence of a static field at the interface. In developing these correlation functions, we are guided by the requirement that the response function in time, *i.e.* the Fourier transform of the frequency domain susceptibility, must be real. [6,90] This implies the final quantity must be either the real or imaginary portion of the complex correlation function – depending on whether the prefactors are purely real or imaginary. [89,90] Thus, a minimum of two correlation functions is required such that their sum or difference necessarily cancels the real or imaginary component of the complex correlation functions that result from grouping the terms in Equation 5.3 and subsequently Fourier transforming to the time domain. Note, in the rotating wave approximation that is commonly invoked in the literature, the response is complex [2, 6] and only agrees with the exact expression in the high frequency limit. [6]

To proceed, it is helpful to restate the following identities and definitions that are used in deriving the new TCF's: [1, 34]

$$i\int_0^\infty dt\, e^{-it(a-ib)} = \frac{1}{a-bi} \tag{5.4}$$

$$i\int_0^\infty dt\, e^{-it(a-ib)} i\int_0^\infty dt'\, e^{-it'(a-ib)} = \frac{1}{(a-bi)^2} \tag{5.5}$$

$$\alpha^{ij}(w) = \sum_{gn} \frac{\mu^i_{gn}\mu^j_{gn}}{(\omega_{ng} - w - i\gamma_{ng})} + \frac{\mu^j_{gn}\mu^i_{gn}}{(\omega_{ng} + w + i\gamma_{ng})} \tag{5.6}$$

$$A(t) = e^{\frac{iHt}{\hbar}} A e^{\frac{-iHt}{\hbar}} \tag{5.7}$$

$$\beta^{ijk}_{mg}(\omega) = \frac{1}{\hbar}\sum_n \left[\frac{\alpha^{ij}_{mn}\mu^k_{ng}}{\omega_{ng} - \omega - i\gamma_{ng}} + \frac{\alpha^{ij}_{ng}\mu^k_{mn}}{\omega_{ng} + \omega + i\gamma_{ng}}\right] \tag{5.8}$$

Equation 5.8 should also be familiar to the reader. It describes the frequency dependent hyperpolarizability, β, derived from the second order polarizability tensor specifically for the case of SVFS. [6, 50, 52]

First, the terms in Equation 5.3 that have denominators that are doubly dependent on the resonant frequency ($\omega_2 = \omega_{IR}$) will be examined.

Combining 2a with 4b:

$$C(\omega_2 = \omega_{IR}) = 2a + 4b = \frac{1}{\hbar^3}\sum_{ngmv} \rho_{gg} \frac{\mu^i_{mg}\mu^h_{vm}}{(\omega_{vg} - \omega_2 - i\gamma_{vg})(\omega_{mg} - \omega_2 - i\gamma_{mg})} *$$

$$\left[\frac{\mu^k_{gn}\mu^j_{nv}}{(\omega_{ng} - \omega_s - i\gamma_{ng})} + \frac{\mu^k_{nv}\mu^j_{gn}}{(\omega_{nv} + \omega_s + i\gamma_{nv})}\right] \tag{5.9}$$

$$C(\omega_2 = \omega_{IR}) = \frac{1}{\hbar^2}\sum_{vmg} \rho_{gg} \frac{\alpha^{kj}_{gv}\mu^h_{vm}\mu^i_{mg}}{(\omega_{vg} - \omega_2 - i\gamma_{vg})(\omega_{mg} - \omega_2 - i\gamma_{mg})} \tag{5.10}$$

Utilizing the integral identity in Equation 5.5 and performing the sum over states, Equation 5.10 can be written as the double half-sided (Fourier-Laplace) transform of a novel TCF:

$$C(\omega_2 = \omega_{IR}) = -\frac{1}{\hbar^2}\int_0^\infty dt\, e^{i\omega_2 t}\int_0^\infty dt'\, e^{i\omega_2 t'} < \alpha^{kj}(t+t')\mu^h(t)\mu^i(0) > \tag{5.11}$$

Introduction of the (off-resonant) static polarizability, α, in Equation 5.10 is not exact. It essentially restricts the index 'v' to the vibrational levels in the electronic ground state. This is an excellent approximation under typical thermal conditions. Equation also assumes that the visible and sum frequency fields are not resonant with an electronic transition as they may be in certain cases, [118] but not a typical SVFS experiment.

Making the same approximations, it is possible to introduce the static polarizability by combination of the remaining doubly resonant terms (1a with 3a, 1b with 4a, and 2b with 3b). The results are given below.

$$A(\omega_2 = \omega_{IR}) = 1a + 3a = \frac{1}{\hbar^2}\sum_{mvg}\rho_{gg}\frac{\mu^i_{gv}\mu^h_{mg}\alpha^{kj}_{vm}}{(\omega_{mv} - \omega_2 - i\gamma_{mv})(\omega_{vg} + \omega_2 + i\gamma_{vg})}$$
$$= \frac{1}{\hbar^2}\int_0^\infty dt\; e^{i\omega_2 t}\int_0^\infty dt' e^{i\omega_2 t'} < \mu^i(0)\alpha^{kj}(t+t')\mu^h(t) > \quad (5.12)$$

$$C(-\omega_2 = -\omega_{IR}) = 1b + 4a = \frac{1}{\hbar^2}\sum_{nvg}\rho_{gg}\frac{\mu^i_{gv}\mu^h_{vn}\alpha^{kj}_{ng}}{(\omega_{ng} + \omega_2 + i\gamma_{ng})(\omega_{vg} + \omega_2 + i\gamma_{vg})}$$
$$= -\frac{1}{\hbar^2}\int_0^\infty dt\; e^{i\omega_2 t}\int_0^\infty dt' e^{i\omega_2 t'} < \mu^i(0)\mu^h(t)\alpha^{kj}(t+t') > \quad (5.13)$$

$$A(-\omega_2 = -\omega_{IR}) = 2b + 3b = \frac{1}{\hbar^2}\sum_{mvg}\rho_{gg}\frac{\mu^i_{mg}\mu^h_{gv}\alpha^{kj}_{vm}}{(\omega_{mg} - \omega_2 - i\gamma_{mg})(\omega_{vm} - \omega_2 - i\gamma_{vm})}$$
$$= \frac{1}{\hbar^2}\int_0^\infty dt\; e^{i\omega_2 t}\int_0^\infty dt' e^{i\omega_2 t'} < \mu^h(t)\alpha^{kj}(t+t')\mu^i(0) > \quad (5.14)$$

Note the TCF's in Equations 5.12 – 5.14 and 5.3 are equivalent classically and represent different ordering of the quantum mechanical operators. Collectively, the doubly resonant portion of $\chi^{(3),RES}_{kjih}$ is then given as a sum of four terms:

$$\chi^{(3),D_{RES}}_{kjih} = \int_0^\infty \int_0^\infty dt\ dt'\ e^{i\omega_2(t'+t)} \{C(t,t') + C(-t,-t')$$

$$-A(t,t') - A(-t,-t')\} \tag{5.15}$$

Notice $A(t,t')$ and $A(-t,-t')$ and $C(t,t')$ and $C(-t,-t')$ are complex conjugates respectively in time; their real and imaginary parts are denoted by subscript R and I respectively. Denoting FT as the full Fourier transform: $FT[A(t,t') = A_R(t,t') + iA_I(t,t')] = A_R(\omega,\omega') + A_I(\omega,\omega')$, *i.e.* their Fourier transforms are real due to the time symmetries of the real and imaginary parts of the TCF's. Expanding the correlation functions into their real and imaginary components facilitates the rewriting of Equation 5.15 in terms of the real part of two different quantum mechanical TCF's. (Note, the leading $\hbar$ dependence of the expression is now shown explicitly, defining the TCF's as, *e.g.* $\tilde{A} = \hbar^2 A$. The tilde TCF's are used for emphasis when the $\hbar$ dependence is informative.):

$$\chi^{(3),D_{RES}}_{kjih}(\omega_{IR}) = -\frac{2}{\hbar^2}\int_0^\infty dt\ e^{i\omega_{IR}t} \int_0^\infty dt'\ e^{i\omega_{IR}t'}[\tilde{A}_R(t,t') - \tilde{C}_R(t,t')] \tag{5.16}$$

Equation 5.16 contains a factor of $\frac{1}{\hbar^2}$, thus the $\hbar \longrightarrow 0$ limit is not straightforward. Further, $\tilde{A}_R(t,t')$ and $\tilde{C}_R(t,t')$ are classically equivalent but must differ starting at order $\hbar^2$ for a well defined classical limit to exist. [17, 36] To proceed, a relationship between the quantum mechanical TCF's A and C must be established. Writing TCF's $A(t,t')$ and $C(t,t')$ in their Heisenberg representation and Fourier transforming to the frequency domain gives:

$$A(\omega,\omega') = \frac{1}{\hbar^2}\sum_{nvg}\frac{e^{-\beta E_g}}{Q_p}\mu^i_{gv}\alpha^{kj}_{vn}\mu^h_{ng}\delta(\omega_{vg}-\omega)\delta(\omega_{vn}-\omega') \tag{5.17}$$

$$C(\omega,\omega') = \frac{1}{\hbar^2}\sum_{nvg}\frac{e^{-\beta E_g}}{Q_p}\mu^i_{gv}\mu^h_{vn}\alpha^{kj}_{ng}\delta(\omega_{vg}+\omega)\delta(\omega_{ng}+\omega') \tag{5.18}$$

In Equations 5.17 and 5.18, Q_p is the partition function. Switch dummy indices in Equation 5.18, and making use of symmetric nature of the real α and μ matrix elements, the frequency domain expressions of A and C can be related *via* detailed balance by a single frequency variable:

$$A(\omega,\omega') = e^{\beta\hbar\omega}C(\omega,\omega') \tag{5.19}$$

Equation 5.19 permits rewriting of Equation 5.16 in terms of a single TCF, $\tilde{C}$:

$$\chi^{(3),D_{RES}}_{kjih}(\omega_{IR}) = -\frac{1}{\hbar^2}\int_0^\infty dt\; e^{i\omega_{IR}t}\int_0^\infty dt'\; e^{i\omega_{IR}t'}$$

$$\int_{-\infty}^{\infty} d\omega\; e^{i\omega t}\int_{-\infty}^{\infty} d\omega'\; e^{i\omega' t'}\left[(e^{\beta\hbar\omega}-1)\tilde{C}(\omega,\omega') + (e^{-\beta\hbar\omega}-1)\tilde{C}(-\omega,-\omega')\right] \tag{5.20}$$

In the classical limit, the exponentials in Equation 5.20 can be Taylor expanded. This cancels a factor of $\hbar$ and allows Equation 5.20 to be written in terms of only the imaginary part of TCF $\tilde{C}$. Using classical simulation techniques, only the (classical limit of the) real part of a complex quantum mechanical TCF can be calculated. Thus, it is necessary to establish a relationship between the real and imaginary components of $\tilde{C}(\omega,\omega')$ that would produce another factor of $\hbar$ in the classical limit. [36] Considering $\tilde{C}(\omega,\omega')$, there is no exact relationship between the real and imaginary parts of $\tilde{C}$.

However, in the case of a strictly time independent static field things simplify considerably. Writing out $\tilde{C}(\omega,\omega')$ in the energy representation, it can be shown that the three point correlation function reduces to a two point correlation function because matrix elements of the static dipole $\mu_{ij} = \langle i|\mu|j\rangle = \mu\;\delta_{ij}$, and collapses one of the sums. All

two point correlation functions have real and imaginary parts that are analytically related by a frequency factor of $tanh$; in this case, the real and imaginary components of TCF $\tilde{C}$ are related in frequency space by: $\tilde{C}_I(\omega) = -tanh(\beta\hbar\omega/2)\tilde{C}_R(\omega)$. [119] Expanding correlation function $\tilde{C}$ in Equation 5.16 into its real and imaginary components, and using this relationship to write the sum of correlation functions in terms of only the real part, results in exact cancellation of all components. Thus, to a good first approximation, while the pathways involving the double resonance represent a distinct physical process, their response is not observed due to total deconstructive interference.

In a real system, an intrinsic static field, due to charged species at the interface, will fluctuate in time about its average value. In that case, one must resort to relating the real and imaginary parts of $\tilde{C}$ for a model system [17, 36] and obtain a general expression in terms of $\tilde{C}_R$ (appropriate for all frequencies when quantum corrected) that also has a well defined classical limit.

Considering a model harmonic system with the dipole and polarizability expanded out to second order in the harmonic coordinate Q (one might also consider an anharmonic oscillator with a linear dipole and polarizability but this contribution is expected to be smaller), [17, 34] where primed quantities represent derivatives with respect to the coordinate:

$$\mu_{ij}^{\nu} = \mu_{\nu}^{o}\delta_{ij} + \mu_{\nu}^{\prime}Q_{ij} + \mu_{\nu}^{\prime\prime}\frac{Q_{ij}^2}{2} \tag{5.21}$$

$$\alpha_{ij}^{\nu,\zeta} = \alpha_{\nu,\zeta}^{o}\delta_{ij} + \alpha_{\nu,\zeta}^{\prime}Q_{ij} + \alpha_{\nu,\zeta}^{\prime\prime}\frac{Q_{ij}^2}{2} \tag{5.22}$$

$$Q_{ij} = \langle i|Q|j\rangle = \left(\frac{\hbar}{2m\Omega}\right)^{1/2}\left[\sqrt{j}\delta_{i,j-1} + \sqrt{j+1}\delta_{i,j+1}\right] \tag{5.23}$$

$$Q_{ij}^2 = \left(\frac{\hbar}{m\Omega}\right)\left[(j+1/2)\delta_{ij} + \sqrt{j(j-1)}\delta_{i,j-2} + \sqrt{(j+1)(j+2)}\delta_{i,j+2}\right] \tag{5.24}$$

The resulting higher order (non-static) terms of this TCF are isomorphic to the 5^{th} order Raman case [36] and similar considerations produce a TCF expression to describe this effect. Note, this contribution is only inseparable from the SVFS signal for components of the "static" field that are slowly varying in time for which $\mathbf{k_{IR}} + \mathbf{k_{vis}} + \mathbf{k_{static}} \approx \mathbf{k_{IR}} + \mathbf{k_{vis}}$. In this case, a contribution from this TCF would be possible.

Next, the remaining singly resonant terms need to be considered. Before introduction of the polarizability is possible, simplification of terms 6a and 7b (5a and 8a) is necessary, and can be accomplished through combination of each with two (one) off-resonant terms – making the same approximation ($\omega_{vis} \approx \omega_s$) used in deriving the normal resonant second order susceptibility correlation function for SVFS. [6] Terms 5a, 6a, 7b, and 8a can then be rewritten as:

$$5a = \frac{1}{\hbar^3}\sum_{ngmv}\rho_{gg}\frac{\mu_{gv}^i\mu_{vn}^h\mu_{nm}^k\mu_{mg}^j}{(\omega_{nm}+\omega_s+i\gamma_{nm})(\omega_{mg}-\omega_{vis}-i\gamma_{mg})(\omega_{vg}+\omega_{IR}+i\gamma_{vg})} \tag{5.25}$$

$$6a = \frac{1}{\hbar^3}\sum_{ngmv}\rho_{gg}\frac{\mu_{gv}^i\mu_{vn}^k\mu_{nm}^h\mu_{mg}^j}{(\omega_{mg}-\omega_{vis}-i\gamma_{mg})(\omega_{ng}-\omega_{vis}-i\gamma_{ng})(\omega_{vg}+\omega_{IR}+i\gamma_{vg})} \tag{5.26}$$

$$7b = \frac{1}{\hbar^3}\sum_{ngmv}\rho_{gg}\frac{\mu_{gv}^j\mu_{vn}^h\mu_{nm}^k\mu_{mg}^i}{(\omega_{mg}-\omega_{IR}-i\gamma_{mg})(\omega_{ng}+\omega_{vis}+i\gamma_{ng})(\omega_{vg}+\omega_{vis}+i\gamma_{vg})} \tag{5.27}$$

$$8a = \frac{1}{\hbar^3}\sum_{ngmv}\rho_{gg}\frac{\mu_{gv}^j\mu_{vn}^k\mu_{nm}^h\mu_{mg}^i}{(\omega_{mg}-\omega_{IR}-i\gamma_{mg})(\omega_{vg}+\omega_{vis}+i\gamma_{vg})(\omega_{nv}-\omega_s-i\gamma_{nv})} \tag{5.28}$$

Combination of 5a with 6a, 5b with 6b, 7b with 8a, and 7a with 8b allows for introduction of the non-resonant polarizability and can now be written respectively as:

$$5a + 6a = \frac{1}{\hbar^2} \sum_{gmv} \rho_{gg} \frac{\mu^i_{gm} \alpha^{kh}_{mv} \mu^j_{vg}}{(\omega_{vg} - \omega_{vis} - i\gamma_{vg})(\omega_{mg} + \omega_{IR} + i\gamma_{mg})} \tag{5.29}$$

$$5b + 6b = \frac{1}{\hbar^2} \sum_{gmv} \rho_{gg} \frac{\mu^i_{gm} \mu^j_{mv} \alpha^{kh}_{vg}}{(\omega_{vg} + \omega_s + i\gamma_{vg})(\omega_{mg} + \omega_{IR} + i\gamma_{mg})} \tag{5.30}$$

$$7b + 8a = \frac{1}{\hbar^2} \sum_{gmv} \rho_{gg} \frac{\mu^j_{gv} \alpha^{kh}_{vm} \mu^i_{mg}}{(\omega_{mg} - \omega_{IR} - i\gamma_{mg})(\omega_{vg} + \omega_{vis} + i\gamma_{vg})} \tag{5.31}$$

$$7a + 8b = \frac{1}{\hbar^2} \sum_{gmv} \rho_{gg} \frac{\alpha^{kh}_{gm} \mu^j_{mv} \mu^i_{mg}}{(\omega_{vg} - \omega_s - i\gamma_{vg})(\omega_{mg} - \omega_{IR} - i\gamma_{mg})} \tag{5.32}$$

In forming Equations 5.29 – 5.32 we have again restricted 'v' to the vibrational levels of the electronic ground state. Using the definition of the hyperpolarizability in Equation 5.8, and the integral identity in Equation 5.4, the sum of singly resonant terms can be written as:

$$\chi^{(3),RES'}_{kjih}(\omega_{IR}) = \frac{2}{\hbar} \int_0^\infty dt\, e^{i\omega_{IR}t}\, \tilde{G}_I(t) \tag{5.33}$$

$$\tilde{G}(t) = \hbar\, G(t) = \langle \beta^{khj}(t) \mu^i(0) \rangle \tag{5.34}$$

It can be shown through detailed balance analysis that the Fourier transform of the real, $G_R(t)$, and imaginary, $G_I(t)$, portions of the TCF are analytically related by a frequency factor: $G_I(\omega) = -tanh(\beta\hbar\omega/2) G_R(\omega)$. (Again, where $G_R(\omega)$ and $G_I(\omega)$ are both real.) Thus, this correlation function has a well defined classical limit.

$$\chi^{(3),RES'}_{kjih}(\omega_{IR}) = \frac{2}{\hbar}\int_0^\infty dt\, e^{i\omega_{IR}t}\,\tilde{G}_I(t)$$
$$= -\frac{2}{\hbar}\int_0^\infty dt\, e^{i\omega_{IR}t}\int_{-\infty}^\infty d\omega\, e^{i\omega t}\tanh\left(\frac{\beta\hbar\omega}{2}\right)\tilde{G}_R(\omega)$$
$$\Rightarrow\ lim_{classical} = -\int_0^\infty dt\, e^{i\omega_{IR}t}\int_{-\infty}^\infty d\omega\, e^{i\omega t}\beta\omega\, G_{Cl}(\omega) \quad (5.35)$$

In Equation 5.35, G_{Cl} is the classical TCF of the system's fluctuating hyperpolarizability and system dipole. Note, in applying the resulting TCF theory, one would proceed to calculate the classical limit of $G_R(t)$, take its Fourier transform, and subsequently quantum correct the result. Constructing a quantum correction scheme is straightforward – as described in our previous work, but typically does not greatly change the lineshapes. [17, 120]

5.4 Methods of Computational Implementation

To construct a spectroscopic model for β, the BSM has been modified. Specifically, tensor hyperpolarizabilities can now be assigned to each atom such that when they interact, they reproduce the equilibrium gas phase hyperpolarizability tensor for a given molecule of interest. [47, 91] This new spectroscopic model is referred to as NSM. The hyperpolarizabilities and their derivatives (dependence on molecular geometry is included explicitly in the new spectroscopic model) can be determined from fits to ES calculations using an appropriate basis set. [121–125] The extended Applequist/Thole like model [6, 19, 38, 43–45, 45, 52, 126–130] that has been constructed gives the effective hyperpolarizability (intrinsic + interaction effects), β^{eff}_{ijk}, as sums over the products of the

isolated and condensed phase polarizability matrix elements of the system. The entire process is analogous to the Applequist/Thole many-body polarization method we use to calculate the polarizability. [47] The computational effort is not significantly increased because the most demanding step is still the iteration of the many-body polarization equations.

Within this formalism, the total effective hyperpolarizability (intrinsic + interaction effects), β_{ijk}^{eff}, is given by: [34, 47]

$$\beta_{ijk}^{eff,\alpha\beta\gamma} = \sum_{n} \beta_{n}^{\zeta\epsilon\mu} \frac{\alpha_{ni}^{eff,\mu\alpha}}{\alpha_n} \frac{\alpha_{nj}^{eff,\epsilon\beta}}{\alpha_n} \frac{\alpha_{nk}^{eff,\zeta\gamma}}{\alpha_n} \tag{5.36}$$

In Equation 5.36, $\beta_{n}^{\zeta\epsilon\mu}$ is the intrinsic hyperpolarizability tensor associated with atom n, $\alpha_{ni}^{eff,\mu\alpha}$ is the total effective polarizability tensor component between atom i and n, and α_n is the intrinsic point polarizability associated with atom n. [47]

The NSM was implemented to develop a model of the system hyperpolarizability for water. To our knowledge, only two experiments [114, 115] that were published in the 1960's have investigated the hyperpolarizability of gaseous water. Given that technological innovations since that time have led to more accurate data in terms of measuring gas phase electric moments, the values obtained from the referenced works were used as a rough guide only. All parametrization for the hyperpolarizability of water was performed using detailed ES calculations with PCGAMESS, and also by comparing to other theoretical investigations. [131]

The equilibrium water configurations along with the polarizability parameters used in the ES and NSM calculations are those detailed previously in Chapter 3. The ES calcula-

tions were done at the aug-cc-pvqz level, and electron correlation was accounted for using B3LYP5. (MP2, used in previous BSM developments, is a valid option for electron correlation when calculating polarizabilities but not hyperpolarizabilities in PCGAMESS. For consistency, it was checked to ensure that B3LYP5 and MP2 produced the same polarizability derivatives. They do.) The hyperpolarizability derivative tensors were obtained *via* the 9 coordinate displacement method detailed in Chapter 3.

First the intrinsic hyperpolarizability tensors of Oxygen and Hydrogen were determined such that when they interacted *via* the NSM, the gas phase hyperpolarizability tensor of water, calculated using PCGAMESS, was reproduced. The best fit intrinsic hyperpolarizability tensors parameters associated with the Oxygen and Hydrogen are presented in Table 5.1. Table 5.1 also compares the interaction hyperpolarizability tensor of a single water molecule computed *via* ES and NSM methods. Agreement between the two methods is remarkable – especially considering previous techniques that are capable of calculating the hyperpolarizability of water on the fly were only able to match ES calculations within a 15% error. [91]

Subsequently, the intrinsic hyperpolarizability derivative tensors of Oxygen and Hydrogen were parametrized. Introduction of the hyperpolarizability derivative tensors allows the total hyperpolarizability to be expressed as a function of both displacement from equilibrium bond length (Δr) and angle ($\Delta\theta$): $\beta^{ijk} = \beta_o^{ijk} + \beta_r'^{ijk}\Delta r + \beta_\theta'^{ijk}\Delta\theta$. Extensive global scan methods were employed in pursuit of finding a composition of the hyperpolarizability derivative tensors for Oxygen and Hydrogen that would model the fluctuations

	$\epsilon_{xxz}\beta^{xxz}$	$\epsilon_{yyz}\beta^{yyz}$	β^{zzz}
O	0.679	-0.271	0.059
H	-0.6725	0.6875	-0.8625
ES	-0.5733135	-0.2205550	-0.6087189
NSM	-0.5733011	-0.2205574	-0.6087125
%Error	-0.0021628655	0.0010881640	-0.0010513884

Table 5.1: The non-zero intrinsic hyperpolarizability tensor parameters of Oxygen and Hydrogen used in the NSM calculations are give below. Following, the non-zero interaction hyperpolarizability tensor elements of an equilibrium configuration isolated water molecule are given for both ES and NSM methods along with their percent error. Note, ϵ symbolizes the hyperpolarizability is fully symmetric with respect to all superscripts.

	$\beta_r'^{xxz}$	$\beta_r'^{yyz}$	$\beta_r'^{zzz}$
O	6.300	-0.650	5.260
H	3.75	37.95	-0.5
	$\beta_\theta'^{xxz}$	$\beta_\theta'^{yyz}$	$\beta_\theta'^{zzz}$
O	3.750	0.	3.0
H	8.933	0.	-35.8

Table 5.2: The hyperpolarizability derivative parameters for the NSM of gaseous water are shown. Units are in $\text{Å}^4/e$ for β_r' and Å^5/($e$radian) for β_θ'.

of all ijk tensor components of the system β, but none where found. However, third order SVFS signals depend only on the system's fluctuations in the total hyperpolarizability in three specific directions: β^{zxz}, β^{xxz}, and β^{zzz}. Further, the most common SVFS measurement is taken in the XXZ direction (because it gives by far the most intense signal). Therefore, while not ideal, it is sufficient to have a model that captures the system's fluctuating hyperpolarizability derivative tensor in the XXZ direction. Table 5.2 gives the non-zero hyperpolarizability derivative tensor parameters for Oxygen and Hydrogen that best reproduced the interaction hyperpolarizability tensor of gaseous water. There were several global fits that reproduced the XXZ component of the interaction hyperpolarizability derivative tensor. The set of parameters that was selected was chosen based upon its ability to also reproduce the two other relevant directions (ZXZ and ZZZ) in the majority of coordinate displacements.

Table 5.3 lists the resultant interaction hyperpolarizability derivative tensor in the XXZ, ZXZ, and ZZX directions calculated using ES and NSM methods. Note, only the derivatives that have an order of magnitude $\geq$E^{-1}Å$^4/e$ in the SVFS relevant directions are given in Table 5.3.

In pursuit of further testing the NSM, the total hyperpolarizability of a water dimer was calculated using both ES and NSM methods. The same coordinate displacement method, detailed previously, was implemented to obtain the polarizability matrix. In this case, 18 displacements were made instead of 9. The results of ES and NSM methods were compared to determine whether the NSM was capable of capturing the influence of the additional interactions affect on the system hyperpolarizability. The XXZ hyperpolarizability derivative tensor element calculated *via* NSM exhibits at most a 2.4% difference from the ES determinations, and this difference is as small as .16%. The ZZZ and ZZX elements are not reproduced as well as the XXZ element. In general, most of the ZZZ and ZZX tensor elements are within a percent difference of 2-3%. However, there are outliers that fall far from the ES value – as high as 139% difference in the ZZX direction.

The model was further tested by assessing its ability to capture the hyperpolarizability tensor components of condensed phase water as compared to two other detailed, ES based, theoretical investigations. [91, 124] The system configurations were generated using CM3D, [132] an MD code developed at the University of Pennsylvania. Microcanonical MD of 64 water molecules was performed at a density of 1.0 g /cm^3 and an average temperature of 298K.

Displacement	Component	ES	NSM	%Difference
Ox:	β'^{zxz}	0.535820	0.536980	0.11598
Oz:	β'^{xxz}	1.371292	1.382532	-0.23294
Oz:	β'^{zzz}	0.866077	0.863747	1.123897
H1x:	β'^{xxz}	-1.34889	-1.34932	-0.0433224
H1x:	β'^{zzz}	-0.491203	-0.491037	0.016639
H1x:	β'^{zzx}	-0.267954	-0.268592	-0.063821
H1z:	β'^{xxz}	-0.685743	-0.691192	-0.54485
H1z:	β'^{zzz}	-0.433137	-0.8431843	0.129398
H1z:	β'^{zzx}	-0.5627319	-2.002802	-144.007
H2x:	β'^{xxz}	1.348770	1.349364	0.059449
H2x:	β'^{zzz}	0.491239	0.49072155	-0.05070
H2x:	β'^{zzx}	-0.26790	-0.268388	-0.04881
H2z:	β'^{xxz}	-0.68574	-0.6911921	-0.54514
H2z:	β'^{zzz}	-0.433117	-0.4318426	0.127441
H2z:	β'^{zzx}	0.562732	2.002801	144.007

Table 5.3: The hyperpolarizability derivative components of gaseous water that are relevant to third order SVFS and non-zero for a given displacement are listed for both ES and NSM calculation methods. The percent error between NSM and ES methods is also listed. Note, the first column designates the coordinate that was displaced as described in the text, and units are in $\text{Å}^4/e$.

The XXZ and YYZ components of the hyperpolarizability tensor compare well with the other ES based theoretical investigations. Specifically, the change of sign that is associated with the hyperpolarizability tensor of water going from the gas phase to the condensed phase is reproduced! Our method calculates β^{XXZ}=0.18 a.u. and β^{YYZ}=10.60 a.u.. Values calculated by Jensen (Kusalik et. al) using various ES techniques fall in the range of β^{XXZ}=0.14-0.81 (4.1-5.7) a.u. and β^{YYZ}=7.5-9.03 (10.9-18.8) a.u.. The β^{ZZZ} component calculated by our model is obviously incorrect – the trademark change of sign is not present in this direction. Our model calculates β^{ZZZ}=-42.175 a.u..

Despite it short comings, the NSM does remarkably well in reproducing the most relevant component to third order SVFS – the XXZ component of the system hyperpolarizability derivative tensor for a water, a water dimer, and condensed phase water. For calculations involving one and two water molecules, the total system hyperpolarizability calculated *via* ES and NSM agree well. For calculations involving condensed phase water, only two of the three non-zero hyperpolarizability tensor components could be reproduced. To date, no other molecularly detailed, on the fly, technique has been able to do as well in reproducing a system's hyperpolarizability, let alone the hyperpolarizability derivatives and for a system as complicated as water! Further investigation and refinement of this model is clearly required, but the initial results are promising. Specifically, because the total system hyperpolarizability is a function of intrinsic and system polarizability elements, it's advisable that the NSM be modified to incorporate an atom's intrinsic polarizability tensor instead of this quantity being approximated as a point polarizability.

Chapter 6

Linear Raman: A Frequency-Time Derivation of the Response Function

Off-resonant Raman experiments employ three individually off-resonant visible fields. [5] The wave vector matching condition and the signal frequency are $\boldsymbol{k}_s = \boldsymbol{k}_1 - \boldsymbol{k}_2 + \boldsymbol{k}_3$ and $\omega_s = \omega_1 - \omega_2 + \omega_3$ respectively. The resonant frequency is at $\omega_1 - \omega_2$, and the signal frequency is off-resonant. In some off-resonant Raman experiments, $\boldsymbol{k}_1 = \boldsymbol{k}_3$. This is not a necessary condition, and thus we treat $\boldsymbol{k}_1$ and $\boldsymbol{k}_3$ to be distinguishable fields.

Starting from corrections to the Schrodinger wavefunction formalism, since no individual field is resonant, [2, 133] and averaging over the initial distribution of states, when all three fields are distinguishable, there are 24 terms that describe the third order susceptibility. For off-resonant Raman, only terms that contain a denominator of the form $(\omega_{ab} \pm \omega_1 \mp \omega_2 \pm i\gamma_{ab})$ will contribute to the resonant polarization. Thus, only eight of the twenty four terms need to be considered when determining the resonant susceptibility.

Starting from Equation 5.2 as the definition of the polarization in terms of its' Cartesian tensor components, and assuming the three fields are all distinguishable, the *resonant* portion of the susceptibility is given by:

$$\chi^{(3)}_{kjih}(\omega_s, \omega_1, -\omega_2, \omega_3) =$$

$$\sum_{gmnv} \frac{-\rho_{gg}}{\hbar^3} \left(+(1d) \frac{\mu^k_{gv}\mu^h_{vn}\mu^i_{nm}\mu^j_{mg}}{(\omega_{vg} - \omega_s - i\gamma_{vg})(\omega_{ng} - \omega_1 + \omega_2 - i\gamma_{ng})(\omega_{mg} - \omega_1 - i\gamma_{mg})} \right.$$

$$+(1e) \frac{\mu^k_{gv}\mu^h_{vn}\mu^j_{nm}\mu^i_{mg}}{(\omega_{vg} - \omega_s - i\gamma_{vg})(\omega_{ng} - \omega_1 + \omega_2 - i\gamma_{ng})(\omega_{mg} + \omega_2 - i\gamma_{mg})}$$

$$+(2d) \frac{\mu^h_{gv}\mu^k_{vn}\mu^i_{nm}\mu^j_{mg}}{(\omega_{vg} + \omega_3 + i\gamma_{vg})(\omega_{ng} - \omega_1 + \omega_2 - i\gamma_{ng})(\omega_{mg} - \omega_1 - i\gamma_{mg})}$$

$$+(2e) \frac{\mu^h_{gv}\mu^k_{vn}\mu^j_{nm}\mu^i_{mg}}{(\omega_{vg} + \omega_3 + i\gamma_{vg})(\omega_{ng} + \omega_2 - \omega_1 - i\gamma_{ng})(\omega_{mg} + \omega_2 - i\gamma_{mg})}$$

$$+(3a) \frac{\mu^j_{gv}\mu^i_{vn}\mu^k_{nm}\mu^h_{mg}}{(\omega_{vg} + \omega_1 + i\gamma_{vg})(\omega_{ng} + \omega_1 - \omega_2 + i\gamma_{ng})(\omega_{mg} - \omega_3 - i\gamma_{mg})}$$

$$+(3b) \frac{\mu^i_{gv}\mu^j_{vn}\mu^k_{nm}\mu^h_{mg}}{(\omega_{vg} - \omega_2 + i\gamma_{vg})(\omega_{ng} + \omega_1 - \omega_2 + i\gamma_{ng})(\omega_{mg} - \omega_3 - i\gamma_{mg})}$$

$$+(4a) \frac{\mu^j_{gv}\mu^i_{vn}\mu^h_{nm}\mu^k_{mg}}{(\omega_{vg} + \omega_1 + i\gamma_{vg})(\omega_{ng} + \omega_1 - \omega_2 + i\gamma_{ng})(\omega_{mg} + \omega_s + i\gamma_{mg})}$$

$$\left. +(4b) \frac{\mu^i_{gv}\mu^j_{vn}\mu^h_{nm}\mu^k_{mg}}{(\omega_{vg} - \omega_2 + i\gamma_{vg})(\omega_{ng} + \omega_1 - \omega_2 + i\gamma_{ng})(\omega_{mg} + \omega_s + i\gamma_{mg})} \right) \tag{6.1}$$

In the following algebraic manipulation, we introduce the static polarizability, α, because all three fields and the signal field fall far from resonance. Formally, introduction of the static polarizability amounts to approximating $\omega_1 \approx \omega_2 \approx \omega_3 \approx \omega_s$:

$$1d + 2d = \frac{1}{\hbar^3} \sum_{mngv} \frac{\mu^i_{nm}\mu^j_{mg}}{(\omega_{ng} - \omega_1 + \omega_2 - i\gamma_{ng})(\omega_{mg} - \omega_1 - i\gamma_{mg})}$$

$$* \left[\frac{\mu^k_{gv}\mu^h_{vn}}{\omega_{vg} - w_s - i\gamma_{vg}} + \frac{\mu^h_{gv}\mu^k_{vn}}{\omega_{vg} + w_3 + i\gamma_{vg}} \right]$$

$$= \frac{1}{\hbar^2} \sum_{mng} \frac{\mu^i_{nm}\mu^j_{mg}\alpha^{kh}_{gn}}{(\omega_{ng} - \omega_1 + \omega_2 - i\gamma_{ng})(\omega_{mg} - \omega_1 - i\gamma_{mg})} \tag{6.2}$$

$$1e + 2e = \frac{1}{\hbar^3} \sum_{mngv} \frac{\mu^j_{nm}\mu^i_{mg}}{(\omega_{ng} - \omega_1 + \omega_2 - i\gamma_{ng})(\omega_{mg} + \omega_2 + i\gamma_{mg})}$$

$$* \left[\frac{\mu^k_{gv}\mu^h_{vn}}{\omega_{vg} - w_s - i\gamma_{vg}} + \frac{\mu^h_{gv}\mu^k_{vn}}{\omega_{vg} + w_3 + i\gamma_{vg}} \right]$$

$$= \frac{1}{\hbar^2} \sum_{mng} \frac{\mu^j_{nm}\mu^i_{mg}\alpha^{kh}_{gn}}{(\omega_{ng} - \omega_1 + \omega_2 - i\gamma_{ng})(\omega_{mg} + \omega_2 + i\gamma_{mg})} \tag{6.3}$$

$$3a + 4a = \frac{1}{\hbar^3} \sum_{mngv} \frac{\mu^i_{mn}\mu^j_{gm}}{(\omega_{ng} + \omega_1 - \omega_2 + i\gamma_{ng})(\omega_{mg} + \omega_1 + i\gamma_{mg})} \tag{6.4}$$

$$* \left[\frac{\mu^k_{nv}\mu^h_{vg}}{\omega_{vg} - w_3 - i\gamma_{vg}} + \frac{\mu^h_{nv}\mu^k_{vg}}{\omega_{vg} + w_s + i\gamma_{vg}} \right]$$

$$= \frac{1}{\hbar^2} \sum_{mng} \frac{\mu^i_{mn}\mu^j_{gm}\alpha^{kh}_{ng}}{(\omega_{ng} + \omega_1 - \omega_2 + i\gamma_{ng})(\omega_{mg} + \omega_1 + i\gamma_{mg})} \tag{6.5}$$

$$3b + 4b = \frac{1}{\hbar^3} \sum_{mngv} \frac{\mu^i_{gm}\mu^j_{mn}}{(\omega_{ng} + \omega_1 - \omega_2 + i\gamma_{ng})(\omega_{mg} - \omega_2 + i\gamma_{mg})}$$

$$\left[\frac{\mu^k_{nv}\mu^h_{vg}}{\omega_{vg} - w_3 - i\gamma_{vg}} + \frac{\mu^h_{nv}\mu^k_{vg}}{\omega_{vg} + w_s + i\gamma_{vg}} \right]$$

$$= \frac{1}{\hbar^2} \sum_{mng} \frac{\mu^i_{gm}\mu^j_{mn}\alpha^{kh}_{ng}}{(\omega_{ng} + \omega_1 - \omega_2 + i\gamma_{ng})(\omega_{mg} - \omega_2 + i\gamma_{mg})} \tag{6.6}$$

Combining Equations 6.2 with 6.3 and 6.5 with 6.6 results in Equations 6.7 and 6.8 respectively.

$$Eq.\ 6.2\ +\ Eq.\ 6.3 = \frac{i}{\hbar}\int_0^\infty dt e^{-it(\omega_2-\omega_1)} < \alpha^{kh}(t)\alpha^{ij}(0) > \tag{6.7}$$

$$Eq.\ 6.5\ +\ Eq.\ 6.6 = -\frac{i}{\hbar}\int_0^\infty dt e^{-it(\omega_2-\omega_1)} < \alpha^{kh}(0)\alpha^{ij}(t) > \tag{6.8}$$

Equation 6.8 is the complex conjugate of 6.7. Their sum is, thus, equal to twice the imaginary portion of the correlation function. Making use of this simplification, the time domain Raman susceptibility tensor, $\chi^{(3),RAMAN}_{kjih}(t)$, is now given by:

$$\chi^{(3),RAMAN}_{kjih}(t) = \frac{2}{\hbar} Im\left\{ < \alpha^{kh}(t)\alpha^{ij}(0) > \right\} \tag{6.9}$$

The imaginary portion of the polarizability autocorrelation function, can be related via the fluctuation dissipation theorem to the real part, and the real part to its' classical analog. [5]

Chapter 7

Conclusion

Spectroscopy is a power tool for investigating the structure and dynamics of chemical systems. A system's spectroscopic response (susceptibility) is formally described by a complex quantum mechanical quantity which appears to have no obvious classical limit. This manuscript has presented mathematical techniques applied to general susceptibility expressions that allow for unique TCF's describing a specific optical process to be derived. These TCF's are shown to have a definitive classical limit, and are thus, amenable to semiclassical computation techniques. The semiclassical computation technique developed and used in this work hinges upon two primary components – classical MD and a spectroscopic model. Specifically, the trajectories generated from classical MD are used as input into the spectroscopic model such that the fluctuations in the system's electric moments and electric moment's derivatives are captured as accurately as possible. Thus, the TCF's that describe a particular type of spectroscopy are able to also be calculated as accurately as possible.

The robust nature of our semiclassical computation technique in calculating spectroscopic observables in a molecularly detailed manner has also been tested. Modeling the spectroscopy of liquid water systems in a molecularly detailed methodology has historically been considered difficult [42, 50, 82, 134–136] due to the strong many-body interactions that are present. The spectroscopic model presented in this manuscript is able to capture the nature of the complex many-body interactions as evidenced by it's ability to reproduce the fine details (subpopulation and phase) of experimental interfacial water spectra. Further, an extension of the spectroscopic model that goes beyond calculating the system's dipole and polarizability moments also has been presented. Preliminary calculations parametrizing the hyperpolarizability and hyperpolarizability fluctuations have also been conducted for a water molecule and a water dimer. Initial results are in good agreement with other theoretical work, and appear to capture the total hyperpolarizability better than any other molecularly detailed on the fly method to date for a condensed phase system.

References

[1] W. Heitler, *The Quantum Theory of Radiation* (Dover Publications Inc., New York, 1984).

[2] R. W. Boyd, *Nonlinear Optics* (Academic Press, London, 2003).

[3] Y. Shen, *Principles of Nonlinear Optics* (Wiley, New York, 1984).

[4] P. Butcher and D. Cotter, *The Elements of Nonlinear Optics* (Cambridge University Press, Cambridge, 1990).

[5] S. Mukamel, *Principles of Nonlinear Optical Spectroscopy* (Oxford University Press, Oxford, 1995).

[6] A. Perry, C. Neipert, B. Space, and P. Moore, Chem. Rev. **106**, 1234 (2006).

[7] G. Richmond, Chem. Rev. **102**, 2693 (2002).

[8] R. Rey, K. B. Moller, and J. T. Hynes, Chem. Rev. **104**, 1915 (2004).

[9] M. T. Zanni, N.-H. Ge, Y. Sam Kim, and R. M. Hochstrasser, PNAS **98**, 11265 (2001).

[10] P. Hamm, M. Lim, W. F. DeGrado, and R. M. Hochstrasser, J. Chem. Phys. **112**, 1907 (2000).

[11] S. Li *et al.*, J. Phys. Chem. B **110**, 18933 (2006).

[12] A. N. Bordenyuk and A. V. Benderskii, J. Chem. Phys. **122**, 134713(1) (2005).

[13] P. Peterson and R. Saykally, Annu. Rev. Phys. Chem. **57**, 333 (2006).

[14] K. Eisenthal, Chem. Rev. **106**, 1462 (2006).

[15] E. Hao, G. Schatz, R. Johnson, and J. Hupp, J. Chem. Phys. **117**, 5961 (2006).

[16] H. Torii, J. Phys. Chem. A **110**, 9469 (2006).

[17] R. DeVane *et al.*, J. Chem. Phys. **121**, 3688 (2004).

[18] R. DeVane, C. Ridley, T. Keyes, and B. Space, J. Chem. Phys. **123**, 194507 (2005).

[19] A. Perry *et al.*, J. Chem. Phys. **123**, 144705(1) (2005).

[20] N. Bloembergen and P. Pershan, Phys. Rev. **128**, 606 (1962).

[21] N. Bloembergen, R. Chang, S. Jha, and C. Lee, Phys. Rev. **174**, 813 (1968).

[22] J. Armstrong, N. Bloembergen, J. Ducuing, and P. Pershan, Phys. Rev. **127**, 1918 (1962).

[23] C. H. Lee, R. K. Chang, and N. Bloembergen, Phys. Rev. Lett. **18**, 167 (1967).

[24] R. G. Gordon, in *Advances in Magnetic Resonance*, edited by J. S. Waugh (Academic Press, New York and London, 1968).

[25] B. J. Berne, M. Tuckerman, J. E. Straub, and A. L. R. Bug, J. Chem. Phys. **93**, 5084 (1990).

[26] R. G. Gordon and R. P. McGinnis, J. Chem. Phys. **55**, 4898 (1971).

[27] R. G. Gordon and R. P. McGinnis, J. Chem. Phys. **49**, 2455 (1968).

[28] M. Alexander and R. G. Gordon, J. Chem. Phys. **55**, 4889 (1971).

[29] R. Gordon, J. Chem. Phys. **43**, 1307 (1965).

[30] P. Adkins and R. Friedman, *Molecular Quantum Mechanics, 3rd Ed.* (Oxford University Press, New York and Oxford, 2001).

[31] R. Silbey, J. Koedijk, and S. Völker, J. Chem. Phys. **105**, 901 (1996).

[32] J. Skinner, Private communication, 2006.

[33] M. Khalil, N. Demirdoven, and A. Tokmakoff, Phys. Rev. Lett. **90**, 047401 (2003).

[34] C. Neipert and B. Space, J. Chem. Phys. **125**, 22406(1) (2006).

[35] R. DeVane *et al.*, Biophys. J. **85**, 2801 (2003).

[36] R. DeVane, C. Ridley, T. Keyes, and B. Space, J. Chem. Phys. **119**, 6073 (2003).

[37] D. A. McQuarrie, *Statistical Mechanics* (Harper and Row, New York, 1976).

[38] A. Perry, H. Ahlborn, P. Moore, and B. Space, J. Chem. Phys. **118**, 8411 (2003).

[39] R. DeVane, C. Ridley, T. Keyes, and B. Space, Phys. Rev. E **70**, 50101 (2004).

[40] G. Herzberg, *Infrared and Raman Spectra of Polyatomic Molecules* (D. Van Nostrand Company, Inc., New York, 1946).

[41] G. Herzberg, *Molecular Spectra & Molecular Structure: Volume I - Spectra of Diatomic Molecules* (D. Van Nostrand Company, Inc., New York, 1946).

[42] C. P. Lawrence and J. L. Skinner, J. Chem. Phys. **117**, 5827 (2002).

[43] B. Thole, Chem. Phys. **59**, 341 (1981).

[44] K. A. Bode and J. Applequist, J. Phys. Chem. **100**, 17820 (1996).

[45] J. Applequist, J. R. Carl, and K.-K. Fung, J. Am. Chem. Soc. **94**, 2952 (1972).

[46] J. Applequist, Acc. Chem. Res. **10**, 79 (1977).

[47] K. Sundberg, J. Chem. Phys. **66**, 114 (1977).

[48] E. A. Raymond, T. L. Tarbuck, and G. L. Richmond, J. Phys. Chem. B **106**, 2817 (2002).

[49] Q. Du, R. Superfine, E. Freysz, and Y. Shen, Phys. Rev. Lett. **70**, 2313 (1993).

[50] A. Morita and J. T. Hynes, J. Phys. Chem. B. **106**, 673 (2002).

[51] R. Kubo, in *Fluctuation, Relaxation and Resonance in Magnetic Systems*, edited by D. T. Haar (Oliver and Boyd, Edinburgh and London, 1961).

[52] A. Perry, C. Neipert, C. Ridley, and B. Space, Phys. Rev. E **71**, 050601(1) (2005).

[53] X. Wei and Y. R. Shen, Phys. Rev. Lett. **86**, 4799 (2001).

[54] J. Wang, Z. Paszti, M. A. Even, and Z. Chen, J. Am. Chem. Soc. **124**, 7016 (2002).

[55] C. Loch, D. Ahn, and Z. Chen, J. Phys. Chem. B **110**, 914 (2006).

[56] M. Hayashi, S. H. Lin, and Y. R. Shen, J. Phys. Chem. A **208**, 8058 (2004).

[57] V. Ostroverkhov, G. A. Waychunas, and Y. R. Shen, Phys. Rev. Lett. **94**, 0461021 (2005).

[58] M. Bonn, H. Ueba, and M. Wolf, J. Phys. Condens. Matter **17**, S201 (2005).

[59] S. Roke, A. W. Kleyn, and M. Bonn, Chem. Phys. Lett. **370**, 227 (2003).

[60] F. Vidal and A. Tadjeddine, Rep. Prog. Phys. **68**, 1095 (2005).

[61] R. Lu *et al.*, J. Phys. Chem. B **108**, 7297 (2004).

[62] R. Kubo, in *Lectures in Theoretical Physics*, edited by W. Britton and L. Dunham (Interscience Publishers Inc., New York, 1959).

[63] B. J. Berne and G. D. Harp, Adv. Chem. Phys. **17**, 63 (1970).

[64] H. Ahlborn, X. Ji, B. Space, and P. B. Moore, J. Chem. Phys. **111**, 10622 (1999).

[65] X. Ji *et al.*, J. Chem. Phys. **112**, 4186 (2000).

[66] K. R. Wilson *et al.*, J. Phys. Cond. Matter **14**, L221 (2002).

[67] K. R. Wilson *et al.*, J. Chem. Phys. **117**, 7738 (2002).

[68] I. W. Kuo and C. J. Mundy, Science **303**, 658 (2004).

[69] R. Braun *et al.*, J. Chem. Phys. **110**, 4634 (1999).

[70] D. K. Hore, M. Y. Hamamoto, and G. Richmond, J. Chem. Phys. **121**, 12589 (2004).

[71] O. Pluchery and A. Tadjeddine, J. Electroanal. Chem. **500**, 379 (2001).

[72] E. A. Raymond and G. L. Richmond, J. Phys. Chem. B **108**, 5051 (2004).

[73] Y. Shen, Private Correspondence.

[74] K. Toukan and A. Rahman, Phys. Rev. B **31**, 2643 (1985).

[75] D. Hore, Private Correspondence.

[76] D. K. H. D. S. Walker and G. L. Richmond, J. Phys. Chem. B **110**, 20451 (2006).

[77] M. J. Shultz, C. Schnitzer, D. Simonelli, and S. Baldelli, Int. Rev. Phys. Chem. **19**, 123 (2000).

[78] T. Tarbuck and G. Richmond, J. Phys. Chem. B **109**, 20868 (2005).

[79] C. Konek *et al.*, JACS **127**, 15771 (2005).

[80] G. Ma and H. Allen, Langmuir **22**, 5341 (2006).

[81] F. Vidal, B. Busson, A. Tadjeddine, and A. Peremans, J. Chem. Phys. **119**, 12492 (2003).

[82] A. Morita, J. Phys. Chem. B **110**, 3158 (2006).

[83] P. Vassilev *et al.*, J. Chem. Phys. **115**, 9815 (2001).

[84] I. Benjamin, Phys. Rev. Let. **73**, 2083 (1994).

[85] X. Wei *et al.*, J. Phys. Chem. B **104**, 3349 (2000).

[86] H. Held, A. I. Lvovsky, X. Wei, and Y. R. Shen, Phys. Rev. B **66**, 2051101 (2002).

[87] A. Morita, Chem. Phys. Lett. **398**, 361 (2004).

[88] X. Wei *et al.*, J. Phys. Chem. B **104**, 3349 (2000).

[89] R. van Zon and J. Schofield, Phys. Rev. E **65**, 011107 (2002).

[90] R. van Zon and J. Schofield, Phys. Rev. E. **65**, 011106 (2002).

[91] L. Jensen, Ph.D. thesis, University of Gorningen, Netherlands, 2004.

[92] I. Yourshaw, Y. Zhao, and D. Neumark, J. Chem. Phys. **105**, 351 (1996).

[93] E. Batista, S. Xantheas, and H. Jonsson, J. Chem. Phys. **109**, 4546 (1998).

[94] A. Buckingham, in *Adv. Chem.Phys. V. 12*, edited by J. Hirschfelder (Interscience Publishers, New York, 1967).

[95] A. D. Lorenzi, A. D. Santis, R. Frattini, and M. Sampoli, Phys. Rev. A **33**, 3900 (1986).

[96] C. Neipert, A. Roney, and B. Space, J. Phys. Chem C **125**, 22406(1) (2007).

[97] R. K. Iler, *The Chemistry of Silica* (Wiley, New York, 1979).

[98] A. P. Legrand, *The Surfaces Properties of Silicas* (Wiley, New York, 1998).

[99] H. Al-Abadleh, A. Mifflin, M. Musorrafiti, and F. Geiger, J. Phys. Chem. B **109**, 16852 (2005).

[100] V. Evangelou, *Environmental Soil and Water Chemistry* (John Wiley and Sons, New York, 1996).

[101] D. Langmuir, *Aqueous Environmental Geochemistry* (Prentic-Hall, New Jersey, 1997).

[102] P. Lopes *et al.*, J. Phys. Chem. B **110**, 2782 (2006).

[103] D. Liu, G. Ma, and H. Allen, Environ. Sci. Technol. **39**, 2025 (2005).

[104] A. Hassanali and S. J. Singer, A model for the water/amorphous silica interface: the undissociated surface, preprint, submitted to J. Phys. Chem. B., 2006, available on the web.

[105] X. L. Zhao, S. Ong, and K. B. Eisenthal, Chem. Phys. Lett. **202**, 513 (1993).

[106] S. Ong, X. L. Zhao, and K. B. Eisenthal, Chem. Phys. Lett. **191**, 327 (1992).

[107] H. Wang, Ph.D. thesis, Columbia University, 1996.

[108] G. Meshulam, Z. Kotler, and G. Berkovic, Opt. Lett. **27**, 1132 (2002).

[109] K. Singer *et al.*, in *Characterization Techniques for Tabulations for Orgainc Nonlinear Optical Materials*, edited by M. Kuzyk and C. Dirk (Marcel Dekker, Inc., New York, 1998).

[110] D. E. Gragson and G. L. Richmond, J. Phys. Chem. B **102**, 569 (1998).

[111] D. Gragson, B. McCarty, and G. L. Richmond, J. Phys. Chem. **100**, 14272 (1996).

[112] P. D. Maker and R. W. Terhune, Phys. Rev. **137**, A801 (1965).

[113] D. E. Gragson and G. L. Richmond, J. Phys. Chem. B **102**, 3847 (1998).

[114] J. L. Levine and T. M. Sanders, Phys. Rev. **154**, 138 (1967).

[115] A. M. Levine, M. Shapiro, and E. Pollak, J. Chem. Phys. **88**, 1959 (1988).

[116] Hanna, Yuratich, and Cotter, *Nonlinear Optics and Free Atoms and Molecules* (Springer-Verlag, Berlin, 1979).

[117] B. Orr and J. Ward, Mol. Phys. **20**, 513 (1971).

[118] M. B. Raschke, M. Hayashi, S. H. Lin, and Y. R. Shen, Chem. Phys. Lett. **359**, 367 (2002).

[119] The -$tanh$ convention was used here to provide clarity with respect to the referenced fifth order Raman theory which also uses the -$tanh$ convention.

[120] H. Ahlborn, B. Space, and P. B. Moore, J. Chem. Phys. **112**, 8083 (2000).

[121] O. Gritsenko, P. Schipper, and E. Baerends, Int. J. Quant. Chem. **76**, 407 (2000).

[122] O. Gritsenko, P. Schipper, and E. Baerends, Chem. Phys. Lett. **302**, 199 (1999).

[123] P. Schipper, O. Gritsenko, S. can Gisbergen, and E. Baerends, J. Chem. Phys. **112**, 1344 (2000).

[124] A. V. Gubskaya and P. G. Kusalik, Mol. Phys. **99**, 1107 (2001).

[125] A. V. Gubskaya and P. G. Kusalik, J. Comp. Meth. Sci. Eng. **4**, 641 (2004).

[126] J. Applequist and C. O. Quicksall, J. Chem. Phys. **66**, 3455 (1977).

[127] B. M. Ladanyi, T. Keyes, D. Tildesley, and W. Street, Mol. Phys. **39**, 645 (1980).

[128] L. C. Geiger, B. M. Ladanyi, and M. E. Chapin, J. Chem. Phys. **93**, 4533 (1990).

[129] D. N. Bernardo, Y. Ding, K. Krogh-Jespersen, and R. M. Levy, J. Phys. Chem. **98**, 4180 (1994).

[130] C. J. Burnham, J. Li, S. S. Xantheas, and M. Leslie, J. Chem. Phys. **110**, 4566 (1999).

[131] L. Jensen, P. T. van Duijnen, and J. Snijders, J. Chem. Phys. **119**, 3800 (2003).

[132] M. Tuckerman, B. J. Berne, and G. J. Martyna, J. Chem. Phys. **97**, 1990 (1992).

[133] When no fields are individually resonant, the density matrix formalism reduces to the same twenty-four terms of the correction to the Schrodinger equation description of nonlinear spectroscopy.

[134] J. B. Asbury *et al.*, J. Phys. Chem. A. **108**, 1107 (2004).

[135] C. P. Lawrence and J. L. Skinner, J. Chem. Phys. **117**, 8847 (2002).

[136] C. P. Lawrence and J. L. Skinner, J. Chem. Phys. **118**, 264 (2003).

About the Author

Christine L. Neipert majored in chemistry and minored in mathematics, receiving a Bachelor's of Science Degree from Maryville University in December of 2002. She entered the Doctoral program, studying computational physical chemistry under Professor Brian Space, at the University of South Florida in January 2003.

In addition to her research and formal coursework, Ms. Neipert attended and made presentations at several national conferences and summer schools. She was also one of nine nationally selected graduate students by Oak Ridge Associated Universities to attend the 2006 Chemistry Nobel Laureates and Students Conference in Lindau, Germany.

While in the Ph.D. program at the University of South Florida, Ms. Neipert was the recipient of the Latino Graduate Fellowship, Tharp Endowed Scholarship, a Department of Energy travel grant, and the Gordon Research Conference Carl Storms travel grant. She was also selected as a National Science Foundation Students-Teachers-and-Researchers graduate fellow, and best oral presentation at the 2006 Castle Conference.